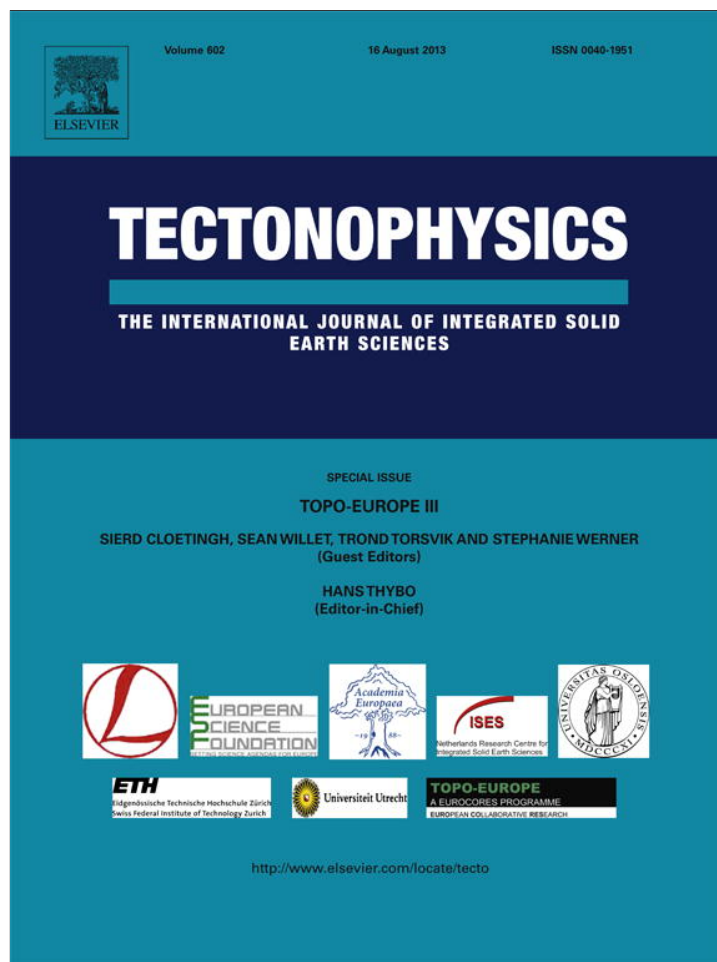


Provided for non-commercial research and education use.  
Not for reproduction, distribution or commercial use.



This article appeared in a journal published by Elsevier. The attached copy is furnished to the author for internal non-commercial research and education use, including for instruction at the authors institution and sharing with colleagues.

Other uses, including reproduction and distribution, or selling or licensing copies, or posting to personal, institutional or third party websites are prohibited.

In most cases authors are permitted to post their version of the article (e.g. in Word or Tex form) to their personal website or institutional repository. Authors requiring further information regarding Elsevier's archiving and manuscript policies are encouraged to visit:

<http://www.elsevier.com/authorsrights>



## Basin evolution in a folding lithosphere: Altai–Sayan and Tien Shan belts in Central Asia

D. Delvaux<sup>a,b,\*</sup>, S. Cloetingh<sup>c</sup>, F. Beekman<sup>c</sup>, D. Sokoutis<sup>c</sup>, E. Burov<sup>d</sup>, M.M. Buslov<sup>e</sup>, K.E. Abdrakhmatov<sup>f</sup>

<sup>a</sup> Royal Museum for Central Africa, Leuvensesteenweg 13, B-3080 Tervuren, Belgium

<sup>b</sup> School of Geosciences, University of the Witwatersrand, Johannesburg, South Africa

<sup>c</sup> Tectonics Group, Dept. of Earth Sciences, Faculty of Geosciences, Utrecht University, The Netherlands

<sup>d</sup> Université Pierre et Marie Curie, ISTEP UMR 7193 UPMC-CNRS, 4 Place Jussieu, 75252 Paris, France

<sup>e</sup> Institute of Geology, SB RAS, Koptyuga ave. 3, Novosibirsk-90, 630090, Russia

<sup>f</sup> Institute of Seismology, National Academy of Sciences, Bishkek, Kyrgyzstan

### ARTICLE INFO

#### Article history:

Received 26 July 2012

Received in revised form 3 January 2013

Accepted 7 January 2013

Available online 24 January 2013

#### Keywords:

Continental lithospheric deformation

Folded lithospheric basins

Tectonic stress

Neotectonics

Central Asia

### ABSTRACT

Central Asia is a classical example for continental lithospheric folding. In particular, the Altai–Sayan belt in South-Siberia and the Kyrgyz Tien Shan display a special mode of lithospheric deformation, involving decoupled lithospheric mantle folding and upper crustal folding and faulting. Both areas have a heterogeneous crust with a long history of accretion–collision, subsequently reactivated as a far-field effect of the Indian–Eurasian collision. Thanks to the youthfulness of the tectonic deformation in this region (peak deformation in late Pliocene–early Pleistocene), the surface expression of lithospheric deformation is well documented by the surface topography and superficial tectonic structures. A review of the paleostress data and tectono-stratigraphic evolution of the Kurai–Chuya basin in Siberian Altai, Zaisan basin in Kazakh South Altai and Issyk–Kul basin in Kyrgyz Tien Shan suggests that they were initiated in an extensional context and inverted by a combination of fault-controlled deformation and flexural folding. In these basins, fault-controlled deformation alone appears largely insufficient to explain their architecture. Lithospheric buckling inducing surface tilting, uplift and subsidence also played an important role. They form typical basins in a folding lithosphere (FLB). Their characteristic basin fill and symmetry, inner structure, folding wavelength and amplitude, thermal regime, time frame are examined in relation to basement structure, stress field, strain rate, timing of deformation, and compared to existing modelling results.

© 2013 Elsevier B.V. All rights reserved.

### 1. Introduction

Both the oceanic and continental lithosphere are known for being able to deform by periodic instabilities, or folding, when submitted to horizontal stresses (Burg et al., 1994; Caporali, 2000; Lefort and Agarwal, 1996; Martinod and Davy, 1994; Sokoutis et al., 2005; Stephenson and Cloetingh, 1991; Zuber, 1987). As soon as the first observations of large lithospheric folds in the oceanic and continental lithosphere have been reported (Stephenson and Lambeck, 1985; Weissel et al., 1980) and the capability of the continental lithosphere to deform with periodic instabilities during compression has been demonstrated theoretically and by analogue modelling (Biot, 1961; Martinod and Davy, 1992), Central Asia became rapidly considered as a type region for large-scale lithospheric folding (Burov and Molnar, 1998; Burov et al., 1993; Nikishin et al., 1993). Since then, lithospheric folding has been recognized as an important mode of basin formation in

compressional intraplate settings in an increasingly number of case studies (Cloetingh et al., 1999, 2002). Recently, Cloetingh and Burov (2011) introduced the concept of Folded Lithospheric Basins (FLB) for the basins that developed in a folding lithosphere. In the meantime, in the type region of Central Asia, knowledge of the tectonic context, time frame, stress field and basin evolution greatly improved. It appears therefore necessary to revisit the geological and geophysical evidence for lithospheric folding and characterize in more details basins developing in a folding lithosphere.

Central Asia is a particularly interesting region for investigating the combination of upper crustal faulting and continental lithospheric buckling thanks to its tectonic youthfulness. The peak of tectonic deformation that caused contractional deformation in the Altai–Sayan and Tien Shan regions in relatively young (late Pliocene–early Pleistocene), as evidenced by structural field work, stress field investigation, magnetic stratigraphy and thermochronology. Thanks to this youthfulness, erosion and sedimentation remained modest and the surface expression of lithospheric deformation is still well documented by the landscape topography and superficial structures.

The intramontane basins of Kurai–Chuya in the Siberian Altai, Zaisan in the Kazakh South Altai and Issyk–Kul in the Kyrgyz Tien Shan

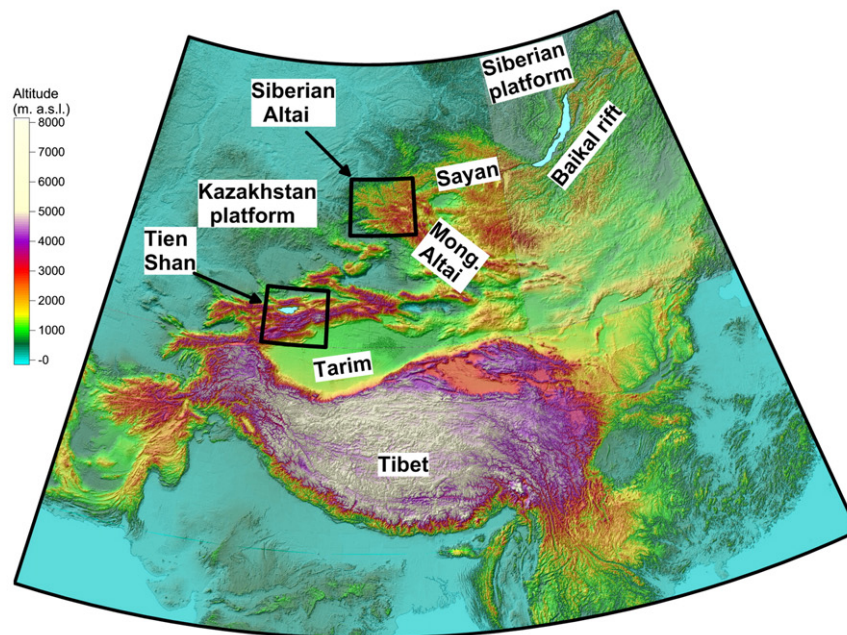
\* Corresponding author at: Royal Museum for Central Africa, Leuvensesteenweg 13, B-3080 Tervuren, Belgium. Tel.: +32 27695426; fax: +32 27695432.  
E-mail address: [damiel.delvaux@africamuseum.be](mailto:damiel.delvaux@africamuseum.be) (D. Delvaux).

developed in a compressional to transpressional context and have been described as ramp or half-ramp basins bounded by thrust faults between rising mountain ranges as documented for the Kurai-Chuya basin system (Buslov et al., 1999; Delvaux et al., 1995c; Thomas et al., 2002), Zaisan basin (Thomas et al., 2002) and Issyk-Kul basin (Chedia, 1986; Cobbold et al., 1993; Sadybakazov, 1990; Thomas et al., 1993).

Detailed field structural and fault kinematic investigations completing recently published results on thermochronology, heat flow,

GPS geodesy, seismic studies and geoelectric sounding provide new constraints that allow re-evaluating the formation mechanisms of these basins. None of the current end-members models for basin development in compressional context (foreland, pull-apart, ramp-type basins) satisfactorily explain the range of observation data. In this paper, we test whether these basins could be better explained by combining lithospheric folding and upper crustal faulting processes in a way proposed for Folded Lithospheric Basins (FLB) by Cloetingh

A



B

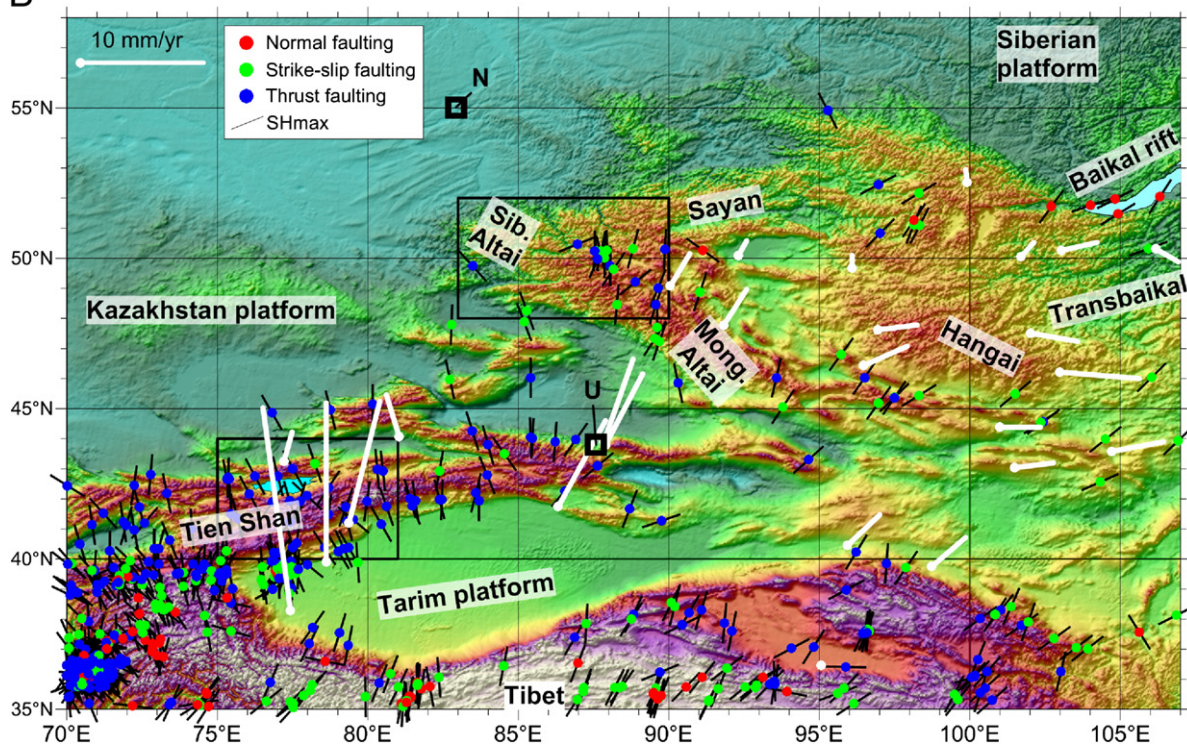


**Fig. 1.** Major structures of Central Asia in (A) Altai–Sayan in South Siberia and NE Kazakhstan and (B) Kyrgyz Tien Shan. Background color in function of elevation (from GTOPO-30). Dots showing location of earthquake focal mechanisms with color in function of type and black lines indicating  $S_{Hmax}$  direction (from Harvard CMTS). White lines with dot mark GPS derived slip vectors. Black squares, Novosibirsk (N) and Urumqi (U) towns.

and Burov (2011). We discuss existing field data and present new observations on these basins within their intraplate Central Asian context, and integrate the recent geophysical results with inferences from analogue and numerical modelling studies.

## 2. Geodynamic setting of Central Asia

Late Cenozoic intracontinental deformation in Central Asia occurs mainly as a distant far-field effect of the India–Eurasia convergence (Fig. 1A). After the initial collision in early Cenozoic, convergence between the two continents continued at a reduced speed (35–40 mm/yr), causing indentation of India into Eurasia (Le Pichon et al., 1992). As a result, the Central Asian mosaic of microplates and mobile belts has been reactivated. The crustal heterogeneity inherited from the Paleozoic to Mesozoic accretion–collision history of the Asian plate localized the deformation into actively deforming belts between weakly deforming rigid blocks. Distribution of seismic epicenter, focal mechanisms, GPS velocity field and geologic slip rates along the major faults confirm the present-day continental deformation in Central Asia in reaction to a strong coupling between Indian and Eurasia (Calais et al., 2006; Vergnolle et al., 2007; Fig. 1B).

### 2.1. Basement formation and thermotectonic age

The wavelength and amplitude of lithospheric folding depend primarily on its stratification and rheology (Burov et al., 1993; Cloetingh and Burov, 2011; Martinod and Davy, 1994; Sokoutis et al., 2005). As a rule of thumb, folding wavelength is proportional to approximately 5–10 thicknesses of the competent layer (Biot, 1961). In the case of a stratified continental lithosphere, superimposed folding wavelengths result from decoupled folding of different competent rheological layers (upper crust and mantle lithosphere; Fig. 2). In the absence of a direct assessment of the stratified rheology, the Effective Elastic Thickness (EET) and the thermotectonic age are used to produce reasonably robust estimates of the integrated lithospheric strength (Cloetingh et al., 1999). In most cases, folding wavelength correlates both with EET and the thermo-tectonic age of the lithosphere. However, EET estimates are more appropriate for lithospheric flexure and thermotectonic age when folding prevails. As this parameter controls primarily the folding wavelength, the geological setting of the Altai–Sayan and Kyrgyz Tien Shan belts is evaluated in terms of thermotectonic age of the lithosphere.

The pre-Cenozoic geodynamic evolution of the Central Asian Orogenic Belt (CAOB) is characterized by progressive continental

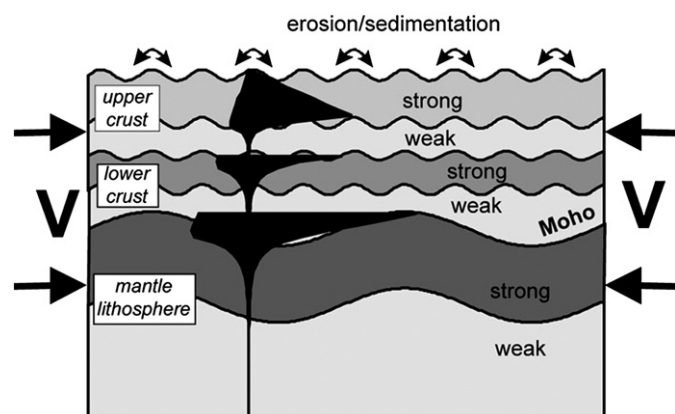


Fig. 2. Schematic concept of folding in a rheologically stratified lithosphere with sedimentation in downfolded areas and erosion of adjacent highs. The rheological stratification of the lithosphere causes different wavelengths of crustal and mantle folding occurring simultaneously (after Cloetingh and Burov, 2011).

growth along the margin of Siberia (Siberian platform and surrounding pre-Neoproterozoic terranes) in a complex succession of paleo-oceanic closure and continental accretion–collision in the late Neoproterozoic–Paleozoic (Berzin et al., 1994; Delvaux et al., 1995b; Dobretsov and Buslov, 2007; Sengör et al., 1993; Windley et al., 2007), and by intracontinental orogeny during the late Paleozoic–Mesozoic (Buslov et al., 2004a, 2004b; De Grave et al., 2007b; Dobretsov et al., 1996).

The basement of the Altai–Sayan region (Fig. 3A) results from a collage of exotic terranes against Siberia during two major Paleozoic collisions (Buslov et al., 2003b, 2004a; Dobretsov and Buslov, 2007; Sengör et al., 1993). Gondwana-derived Altai–Mongolia–Tuva composite microcontinent of Vendian–Cambrian age collided with active margin units of Siberia in the late Devonian–early Carboniferous along the Charych–Terekta–Sayan suture zone. In late Carboniferous–Permian, East Europe and Kazakhstan collided with Siberia along the Chara ophiolite belt, developing in the Altai region a network of strike–slip fault zones. The most important of them are the Irtysh sinistral shear zone (peak activity at 340–320 Ma; Glorie et al., 2012) and its companion North-Eastern shear zone (Buslov et al., 2004b). This was followed in late Permian–Triassic by large magmatic intrusions, building extensive igneous complexes (Dobretsov and Vladimirov, 2001). The crustal structure of the Altai region is therefore highly heterogeneous, with blocks of different thermotectonic ages separated by major shear zones. At the margin of Siberia, the oldest blocks (Kuznetsk Alatai, West Sayan and Gorny Altai) are of Vendian–Cambrian age, intruded by late Ordovician–early Silurian granitoids (e.g. De Grave et al., 2009). Their thermotectonic age is estimated at ~450 Ma. Towards the southwest, these old blocks are surrounded by successively younger crustal fragments of Ordovician to Devonian age (Altai–Mongolia) and Carboniferous age (Rudny Altai and Kalba–Narym), affected by late Carboniferous (300 Ma) to early Jurassic (200 Ma) deformation and magmatism. For them, we estimate a 200–300 Ma thermotectonic age. To the north–west, the Altai belt is bordered by the Barnaul–Biisk basin which is underlain by a Proterozoic basement (Sengör et al., 1993), with a > 600 Ma thermotectonic age.

The Tien Shan lithosphere (Fig. 3B) also formed by successive continental collisions in the Paleozoic, with an important collision stage in late Ordovician and final closure of the Turkestan paleo-ocean in middle Carboniferous to Early Permian (Allen et al., 1992; Carroll et al., 1995; De Grave et al., 2007a, 2011; Glorie et al., 2011). Collision between the Central Tien Shan and the Tarim platform was terminated in late Paleozoic (Gao et al., 2011). North of the Tien Shan, the Kazakhstan platform is composed of terranes accreted and consolidated during Ordovician (Mossakovsky and Dergunov, 1985). Its southern margin corresponds to the Jungar–Balkhach oceanic basin which closed in late Ordovician, consolidated in late Silurian, and was reworked in late Paleozoic (Sengör et al., 1993). The thermotectonic age of the Kazakhstan Platform therefore ranges from Ordovician (480–450 Ma) in its center to late Carboniferous (300 Ma) along its margin.

Some parts of the Tien Shan were affected by later thermal events. Late Triassic to early Cretaceous reactivation of Paleozoic structures is recorded throughout the Tien Shan as the result of the Cimmeride collision further south (De Grave et al., 2007a). In particular Jurassic rejuvenation might have resulted in re-heating of the lithosphere in northwest Tien Shan (Burtman, 1975; Hendrix et al., 1992), Tadjik depression (Leith (1985), Ferghana valley (Schwartzman, 1991). For the latter, this is attested also by low EET values (Burov and Kogan, 1990; Burov et al., 1990).

The Kazakhstan platform is separated by the Chon–Kemin–Chilik fault zone from the North Tien Shan which is of Precambrian origin but intensely affected by Ordovician intrusions (the Issyk–kul microcontinent of Buslov et al., 2003a). The Nikolaev line suture separates it from the Central Tien Shan Devonian–Carboniferous belt. South of the Tien Shan, the Tarim platform has an Archean to early Neoproterozoic basement, covered by unmetamorphosed Riphean–Vendean carbonates, tillites and sandstones, and Phanerozoic

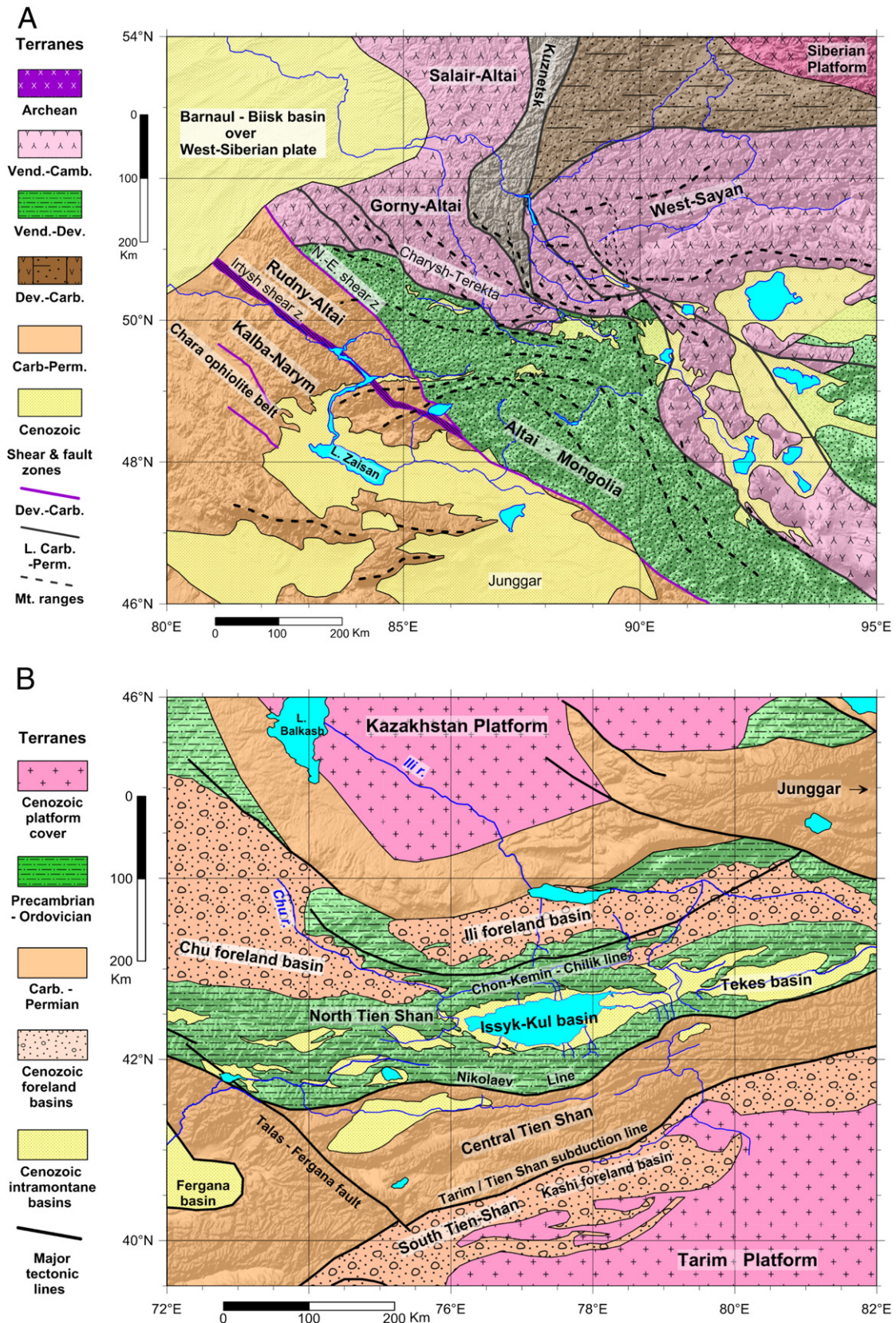


**Fig. 3.** Terrane assemblage and basement tectonic structure of Altai–Sayan (A) and Tien Shan (B). (Compiled respectively from Buslov et al., 2003b, 2004a, 2004b; De Grave et al., 2009; Dobretsov and Buslov, 2007; Kalinin and Moiceeva, 1975; Pubellier, 2008 and from Buslov et al., 2003a, 2007; De Grave et al., 2007a; Omuraliev, 1979, 1980; Pubellier, 2008; Tursungasiev and Petrov, 2008).

sequences totalling 17 km in the major depocenters to 5 km at the margin (Brezhnev, 1995). Its thermotectonic age is estimated at 750 Ma.

The thermotectonic age structure of the Tien Shan belt and adjacent Kazakhstan platform is therefore characterized by alternating belts affected by Ordovician tectonism (~450 Ma) and Devonian to

middle Carboniferous tectonism with late Permian granite intrusions (300–250 Ma), separated by major E–W to ENE–WSW tectonic lines.

## 2.2. Mesozoic–Tertiary intraplate evolution

The timing of the late Cenozoic propagation of tectonic activation in Central Asia received particular interests in terms of basins analysis, magneto-stratigraphy and apatite-fission track (AFT) thermochronology (Abdrakhmatov et al., 1996; De Grave and Van de Haute, 2002; De Grave et al., 2007a; Glorie et al., 2011; Jolivet et al., 2007; Van der Beek et al., 1996; Vassallo et al., 2007; Yuan et al., 2006). The large Central Asian region from the Tien Shan to South-West Tibet and the Baikal rift zone, including Siberian and Mongolian Altai, appears to have a remarkably similar thermo-tectonic evolution for most of the Mesozoic and Cenozoic. This wide region has been affected by a major AFT-inferred Mesozoic cooling phase in the late Cretaceous, followed by a long late Cretaceous–Paleogene period of stability, and a late Cenozoic fast cooling.

In Altai–Sayan as well as in Transbaikalian further east, late Jurassic–early Cretaceous cooling was driven by the final closure of the Mongol–Okhotsk Ocean and subsequent orogenic collision (Delvaux et al., 1995b). In the Tien Shan, Jurassic to early Cretaceous AFT-inferred cooling occurred in response to an important phase of tectonic reactivation, linked to the subduction of the Tethyan lithosphere beneath the southern margin of Tibet and subsequent Cimmeride orogenic collision (De Grave et al., 2007a; Glorie et al., 2011). Since then and until late Cenozoic, this wide intracontinental region remained remarkably stable as shown by the lack of sediments from that period and the very slow cooling rates deduced from the apatite fission track thermal history models. This occurred under predominantly warm and humid conditions, leading to the development of a prominent flat erosion surface, with thick kaolinite-gibbsite and laterite-bauxite weathering profiles (Kashik and Mazilov, 1994). It was interrupted in Oligocene by the onset of basin formation in extensional to transtensional context over a large part of Central Asia (Kurai-Chuya, Zaisan and Issyk-Kul basins; Deviatkin, 1981; Delvaux et al., 1995c; Thomas et al., 2002), a small reheating period due to local volcanism in the Tien Shan (De Grave et al., 2007a), and the onset of sedimentation and volcanism in the Baikal rift zone (Logatchev, 1993). Except for the Baikal region, relative stability persisted until late Cenozoic (De Grave et al., 2007a, 2007b).

## 2.3. Late Cenozoic tectonic activation

Stratigraphic, structural and thermal data show that building of the modern Tien Shan began in mid-Miocene, between 11 and 15 Ma ago, and accelerated in early Pliocene, ~7–5 Ma ago (Bullen et al., 2001, 2003; De Grave et al., 2007a; Glorie et al., 2011; Li et al., 2011; Sun et al., 2004). In Northwest Tien Shan, basin analysis shows that intense tectonism started 7–10 Ma ago (Fang et al., 2007). A cooling event at 20–10 Ma was recorded in the Kalpin uplift at the northwestern edge of the Tarim basin and interpreted as of tectonic origin (J. Chang et al., 2012), but Vinnik et al. (2004) showed that this uplift can be caused by a recent thermal event in the upper mantle. In the Siberian and Mongolian Altai (Fig. 1B), the onset of relief rejuvenation trough mountain building appears slightly younger (5–3 Ma) (Buslov et al., 1999; De Grave et al., 2007a, 2007b; Delvaux et al., 1995c; Vassallo et al., 2007).

This particular thermo-tectonic evolution and young age of mountain building over a large part of Central Asia has important consequences for the preservation of the topographic expression of lithospheric folding. Large-scale undulations of the lithosphere cannot be preserved for much more than 10 Ma after the cessation of compression (Cloetingh and Burov, 2011; Cloetingh et al., 1999). This is due to gravity-driven crustal flow and the action of surface processes trough erosion, transport and redeposition.

The prominent large scale erosion surface which has been stable for almost 150 Ma has been disturbed in a significant way only during the last few million years. Thanks to the relatively dry climate of Central Asia during the glacial periods, the tectonic morphology has been relatively well preserved and can still be observed as flat-topped summits in the Gobi-Altai, Altai and Tien Shan ranges (Cunningham, 2001; Jolivet et al., 2007; Novikov et al., 1998). The presence of elevated well preserved summit plateaus instead of rugged mountain ranges constitutes a unique and useful feature as they represent pre-deformation reference surface on the basis of which the recent (<5 Ma) large-scale crustal deformation can be investigated. These flat summits which are interpreted as representing fragments of the former peneplain and have been widely used in the Russian literature for inferring the neotectonic crustal deformation, described as vertical differential block movements and basement folding (e.g. Chedia, 1986; Deviatkin, 1981; Makarov, 2012).

## 2.4. GPS velocity field

GPS deformation field in Asia shows that convergence between India and Eurasia occurs at 38 mm/yr relative to stable Eurasia along a SSW–NNE profile from Central Tibet to the Altai (Calais et al., 2006). About 20 mm/yr shortening are accommodated in the Himalayas between India and the Tarim basin while the rest is accommodated between the Tarim basin and the Kazakhstan and Siberia platforms. The remaining is distributed laterally with up to 17 mm/yr in Tien Shan and 10–12 mm/yr in Altai (Fig. 1B).

For the Altai belt, GPS-derived velocities with respect to Eurasia along a S–N profile (Fig. 1B) decrease northwards from 10–12 mm/yr at Urumqi, north of the Tien Shan, to ~4 mm/yr in the Altai range and almost zero at Novosibirsk on the Siberian platform (Calais et al., 2003; Goldin et al., 2005). Similarly, GPS-derived shortening rates for the Tien Shan with respect to the Kazakhstan platform shield decrease rapidly from 10–15 mm/yr in South Tien Shan to negligible values along the Kazakhstan platform, over a distance of less than 200 km, along a S–N line passing by the Issyk-Kul depression (Abdrakhmatov et al., 1996; Reigber et al., 2001; Tychkov et al., 2008).

## 2.5. Lithospheric structure

For the Altai–Sayan region, seismic zoning (Dergachev, 2008), heat flow (Duchkov and Sokolova, 1974; Sokolova and Duchkov, 2008), seismotectonic constraints on stress field and geodetic deformation (Babichev et al., 2009; Goldin and Kuchai, 2007; Timofeev et al., 2006; Zhalkovskii et al., 1995) are relatively well documented. The crustal structure (Egorov and Chistyakov, 2003) and upper mantle seismic anisotropy (Dricker et al., 2002) received less attention. The recent heat flow data of Sokolova and Duchkov (2008) confirm earlier observations that the Cenozoic Altai–Sayan is a rather “cold” orogen with an average of 45–50 mW/m<sup>2</sup>, suggesting that neotectonic activity in the area did not cause a temperature increase and is possibly driven by the intraplate tectonic stresses.

While the lithospheric structure of the Siberian Altai is still poorly known, the structure of the central Tien Shan in Kyrgyzstan has been the focus of detailed studies combining heat flow, GPS geodesy, seismological and geoelectric investigations. The Moho depth progressively deepens northwards under the Tien Shan from 45–50 to 60 km, with a 16–25 km thick upper brittle part and a 30–35 km ductile lower part (Bragin et al., 2001). In combination to crustal shortening, Bagdassarov et al. (2011) used xenoliths to show that the Tien Shan lithosphere thickened by an average of 25 ± 5 km since the onset of shortening, 20–30 Ma ago. Combining electric resistivity patterns with gravity field, Bragin et al. (2001) and Tychkov et al. (2008) indicate the presence of a Moho 5–7 km deeper beneath Lake Issyk-Kul than under the neighboring areas. The tomographic models of Bushenkova et al. (2002) show the presence of a high-velocity zone beneath the lake, suggesting a cold lithosphere between 130 and 230 km deep.

**Table 1**

Paleostress results for Eocene–Oligocene (a), late Pliocene–early Pleistocene (b), middle Pleistocene–Holocene (c). N: number of data used; Nt: total number of measured data;  $\sigma_1$ ,  $\sigma_2$ ,  $\sigma_3$ : stress axes; pl: plunge, az: azimuth; R: stress ratio;  $S_{Hmax}$ : horizontal maximum compressional axes; R': stress regime index; Reg: stress regime; quality factor (A: excellent, B: good, C: medium, D: bad). Data source: (1) Delvaux et al., 1995a; (2) Delvaux et al., 1995c; (3) Dehandschutter, 2001; (4) Dehandschutter et al., 2002; (5) Glorie et al., 2012; (6) new data.

Site	Location		Data		$\sigma_1$		$\sigma_2$		$\sigma_3$		R	Misfit angle	$S_{Hmax}$	Regime		QR	Data source
	Long	Lat	N	Nt	pl	az	pl	az	pl	az				R'	Reg.		
<b>a</b>																	
<i>Eocene–Miocene</i>																	
<i>Altai–Sayan</i>																	
AL046	87.625	50.369	15	119	36	297	51	88	14	197	0.85	13.0	108	1.15	SS	D	6
AL223	88.381	50.072	29	32	81	237	2	132	9	42	0.20	10.6	130	0.20	NF	A	6
AL110	88.467	50.117	12	41	54	13	9	272	35	175	0.66	8.3	80	0.66	U	C	6
AL208	88.225	50.034	18	77	83	327	5	105	5	195	0.69	8.1	105	0.69	NF	B	6
AL225	88.067	49.833	9	57	57	127	28	271	16	10	0.34	7.4	110	0.34	NF	D	6
AL237	88.017	49.783	13	41	41	332	44	118	18	226	0.32	7.5	145	1.68	NS	D	6
			96											0.79			
<i>Tien-Shan</i>																	
TS08	76.387	42.623	32	40	69	202	10	84	18	351	0.32	12.3	72	0.32	NF	C	6
CO99-05B	78.034	42.250	11	15	6	291	56	193	34	24	0.72	9.2	114	1.28	SS	D	6
			43											0.80			
<b>b</b>																	
<i>Late Pliocene–Pleistocene</i>																	
<i>Altai–Sayan</i>																	
AL01-04	85.881	50.301	19	23	39	320	2	228	51	136	0.45	5.5	144	2.45	U	C	6
AL01-08	85.645	50.282	17	29	32	104	55	258	12	6	0.35	7.8	101	1.65	SS	C	6
AL01-17	85.736	50.346	18	21	24	323	26	65	53	195	0.30	8.6	138	2.30	TF	C	6
AL01-21	88.301	50.062	7	9	1	161	89	305	0	251	0.16	8.1	161	1.84	SS	D	6
AL01-29	88.375	49.525	28	42	4	338	76	82	14	247	0.58	7.0	157	1.42	SS	B	6
AL46	87.625	50.369	64	119	17	173	8	265	71	17	0.64	11.4	168	2.64	TF	A	2
AL05	87.670	51.750	27	32	12	183	10	90	75	323	0.03	7.2	3	2.03	TF	A	1
AL05	87.670	51.750	46	86	6	180	18	88	71	287	0.17	12.1	0	2.17	TF	A	1
AL111	88.599	50.088	73	129	0	9	6	279	84	101	0.62	14.0	9	2.62	TF	A	2
AL172	87.850	51.360	42	65	14	174	76	360	1	264	0.04	11.1	174	1.96	SS	A	4
AL212	88.541	50.071	17	19	5	30	3	120	84	249	0.34	8.2	30	2.34	TF	C	6
AL213	88.656	50.058	22	263	11	197	21	291	66	81	0.02	8.7	17	2.02	TF	C	6
AL248a	88.450	50.100	28	33	15	199	4	290	75	35	0.10	11.3	19	2.10	TF	A	6
AL248b	88.455	50.105	27	48	5	27	1	110	85	225	0.60	13.3	27	2.60	TF	B	6
AL248b	88.455	50.105	19	48	25	205	5	112	65	12	0.27	8.8	26	2.27	TF	B	6
KZ14b	84.118	49.297	20	73	12	167	72	299	13	74	0.22	5.0	166	1.78	SS	D	5
KZ17-20	84.571	49.096	31	34	8	335	76	97	12	243	0.08	8.8	155	1.92	SS	C	5
KZ21	83.983	49.395	14	54	27	360	1	268	63	176	0.40	9.4	1	2.40	TF	D	5
KZ25	85.404	74.269	30	38	5	308	17	216	72	54	0.51	14.5	129	2.51	TF	A	6
KZ28	85.370	47.244	34	78	4	301	0	31	86	121	0.77	7.2	121	2.77	TF	A	6
KZ30	85.377	47.343	21	85	23	169	9	75	66	325	0.52	13.1	174	2.52	TF	C	6
KZ47	85.411	47.436	24	42	26	146	16	48	59	290	0.33	9.8	151	2.33	TF	B	6
KZ49	85.499	47.399	7	26	22	150	4	58	67	316	0.34	6.3	151	2.34	TF	C	6
KZ51	85.521	47.426	8	8	0	132	12	41	78	225	0.50	1.8	132	2.50	TF	B	6
Tel089	87.600	51.770	21	25	13	359	1	89	77	182	0.42	7.8	179	2.42	TF	A	4
Tel 093	87.680	51.410	18	28	9	165	80	12	5	256	0.49	15.2	165	1.51	SS	B	4
Tel122	87.410	51.48	13	28	25	183	60	37	15	280	0.12	16.1	4	2.12	TF	C	4
TUV01	93.143	53.048	20	26	12	7	77	166	5	276	0.39	3.1	7	1.61	SS	C	3
TUV02	93.231	52.983	11	16	14	18	75	220	5	109	0.60	0.8	19	1.40	SS	C	3
TUV04	93.263	52.871	7	12	37	187	52	23	8	283	0.39	3.1	10	1.61	SS	D	3
TUV08	94.845	50.393	11	11	84	129	1	28	5	297	0.50	3.1	27	0.50	NF	A	3
TUV09	94.433	50.243	9	10	2	195	82	84	7	285	0.59	5.6	15	1.41	SS	B	3
TUV11	94.556	50.233	13	16	77	346	13	161	2	251	0.25	7.1	162	0.25	NF	B	3
TUV25	94.624	51.029	7	38	7	198	37	102	52	298	0.57	9.7	21	2.57	U	B	3
TUV46	89.783	52.167	13	16	26	347	64	165	2	257	0.24	9.7	167	1.76	SS	C	3
TUV49	89.869	52.329	9	11	5	352	53	255	37	86	0.52	9.6	174	1.48	SS	D	3
			795														
<i>Tien Shan</i>																	
CO00-03	75.803	42.530	20	21	17	302	14	207	67	80	0.33	5.4	124	2.33	TF	C	6
CO00-05	77.381	42.083	27	30	4	153	10	36	79	262	0.52	8.9	154	2.52	TF	B	6
CO00-07	77.141	42.146	17	20	16	301	5	33	73	141	0.51	13.4	119	2.51	TF	C	6
CO00-08	77.125	42.141	18	30	0	291	67	203	23	21	0.32	8.2	111	1.68	SS	C	6
CO98-134	75.968	42.689	26	31	17	199	67	338	15	104	0.75	7.8	15	1.25	SS	C	6
CO98-136	76.863	42.067	46	55	21	312	62	175	17	49	0.64	10.3	136	1.36	SS	C	6
CO98-155	75.837	42.631	12	55	26	331	42	88	36	221	0.44	6.6	143	1.56	U	D	6
CO99-13	77.117	42.117	17	37	8	315	52	54	37	219	0.62	6.1	132	1.38	SS	C	6
CO99-21	76.925	42.136	25	64	1	176	1	86	89	311	0.42	8.6	176	2.42	TF	C	6
CO99-22	77.008	42.167	23	41	4	176	84	304	8	85	0.09	10.6	176	1.91	SS	C	6
CO99-25a	76.677	42.202	21	41	4	175	86	6	1	265	0.60	10.2	175	1.40	SS	C	6
CO99-37	76.983	42.083	12	14	13	145	11	52	73	282	0.06	7.9	145	2.06	TF	C	6
CO99-50	77.174	42.147	22	39	5	302	1	212	85	114	0.23	11.1	122	2.23	TF	B	6

(continued on next page)

Table 1 (continued)

Site	Location		Data		$\alpha 1$		$\alpha 2$		$\alpha 3$		R	Misfit angle	$S_{Hmax}$	Regime		QR	Data source
	Long	Lat	N	Nt	pl	az	pl	az	pl	az				R'	Reg.		
<b>b</b>																	
<i>Late Pliocene–Pleistocene</i>																	
Tien Shan																	
CO99-51	75.883	42.656	21	55	12	316	19	222	67	78	0.40	8.2	138	2.40	TF	C	6
TS09	76.385	42.688	29	41	6	156	12	65	76	272	0.33	12.4	157	2.33	TF	C	6
TS11a	76.834	42.636	46	63	23	127	4	35	67	296	0.28	10.3	128	2.28	TF	B	6
TS13	76.627	42.846	16	17	6	316	6	225	82	93	0.09	6.3	136	2.09	TF	C	6
TS16	76.588	42.875	25	36	8	108	8	199	79	334	0.24	17.5	108	2.24	TF	D	6
			423														
<b>c</b>																	
<i>Middle Pleistocene–Holocene</i>																	
Altai																	
AL02	87.300	51.792	18	20	83	198	3	317	6	48	0.73	9.4	138	0.73	NF	A	1
AL03	87.750	51.417	13	13	87	87	3	202	3	292	0.10	0.8	22	0.10	NF	A	1
AL112	88.324	50.066	70	79	86	271	3	100	1	10	0.32	8.3	100	0.32	NF	A	2
AL122	87.410	51.480	14	28	63	168	24	016	11	281	0.50	11.5	7	0.50	NF	B	4
AL128	88.216	49.986	40	46	60	4	30	182	1	272	0.47	11.3	2	0.47	NF	C	2
AL130	88.124	49.944	30	38	6	41	81	171	7	311	0.76	9.0	40	1.24	SS	A	2
AL172	87.850	51.360	12	65	22	334	20	73	59	202	0.48	6.4	146	2.48	TF	B	4
GA03	89.336	50.746	16	16	11	5	8	97	76	221	0.42	6.5	4	2.42	TF	B	3
GA04	89.293	50.757	18	21	1	13	2	103	88	257	0.42	8.9	13	2.42	TF	B	3
GA1-2-7	89.048	50.590	9	11	1	201	5	291	85	103	0.37	6.5	21	2.37	TF	D	3
GA13	88.194	50.923	17	35	23	192	67	9	1	102	0.58	0.9	12	1.42	SS	C	3
GA14	88.190	50.930	14	29	16	210	6	118	72	6	0.17	4.8	30	2.17	TF	C	3
GA16-18	88.098	50.973	14	25	8	228	65	119	23	322	0.14	11.5	48	1.86	SS	C	3
GA20	88.067	51.000	13	17	16	208	62	331	22	111	0.35	5.9	26	1.65	SS	C	3
GA04B-C	89.293	50.757	5	24	10	347	80	177	2	75	0.53	6.2	167	1.47	SS	E	3
GA05-6	89.432	50.669	15	24	4	21	31	114	58	285	0.69	10.5	18	2.69	TF	B	3
GA08-10	88.814	50.586	25	39	7	153	77	274	11	62	0.27	7.1	153	1.73	SS	B	3
KZ43	85.156	48.192	19	25	8	147	1	57	82	322	0.26	6.4	147	2.26	TF	A	6
SH10	88.250	51.370	9	9	24	215	57	82	21	316	0.32	6.6	38	1.68	U	E	3
SH11	88.410	51.420	14	16	30	217	4	309	59	46	0.09	8.3	37	2.09	TF	D	3
Tel058	87.733	51.417	11	50	1	36	83	134	7	306	0.48	4.8	36	1.52	SS	B	4
Tel117	87.830	51.350	27	37	1	207	64	117	26	298	0.10	10.8	27	1.90	SS	A	4
			423														
Tien Shan																	
CO00-04	75.783	42.450	14	15	58	286	25	147	18	49	0.82	11.6	137	0.82	NF	C	6
CO00-06	77.304	42.178	17	20	19	357	7	89	70	199	0.34	5.7	176	2.34	TF	C	6
CO98-155	75.837	42.631	24	55	9	6	64	114	24	272	0.15	14.4	6	1.85	SS	C	6
CO98-157	75.890	42.685	20	33	14	17	1	107	76	202	0.42	7.8	17	2.42	TF	B	6
CO98-54	73.579	41.198	21	34	3	347	1	77	87	182	0.71	10.0	167	2.71	TF	C	6
CO98-79b	76.209	42.718	17	42	28	19	53	244	22	122	0.47	5.9	25	1.53	U	B	6
CO98-97	76.578	42.855	48	65	22	189	68	9	0	99	0.50	14.2	9	1.50	SS	C	6
CO99-21	76.925	42.136	24	64	32	73	58	254	1	164	0.68	11.6	74	1.32	SS	C	6
CO99-22	77.008	42.167	8	41	5	223	4	133	84	6	0.16	6.0	43	2.16	TF	D	6
CO99-22	77.008	42.167	18	23	70	323	18	173	9	80	0.22	10.0	162	0.22	NF	B	6
CO99-25b	76.677	42.202	7	30	21	165	10	259	66	12	0.62	5.6	157	2.62	TF	D	6
CO99-50	77.174	42.147	11	39	15	359	1	89	75	182	0.36	13.3	179	2.36	TF	D	6
CO99-51	75.883	42.656	16	55	18	166	72	346	0	76	0.56	8.4	166	1.44	SS	D	6
CO99-54	77.623	42.805	37	70	34	53	15	154	51	264	0.62	13.5	26	2.62	U	C	6
CO99-56a	77.365	42.838	90	160	1	186	68	278	22	96	0.30	13.1	6	1.70	SS	C	6
CO99-56b	77.367	42.838	29	160	21	206	69	27	1	296	0.04	9.9	26	1.96	SS	D	6
TS11b	76.804	42.629	27	33	19	181	7	273	70	23	0.70	11.7	173	2.70	TF	B	6
TS14	76.634	42.849	28	34	10	351	2	82	80	179	0.18	11.6	171	2.18	TF	C	6
			456														

South of the lake, a low-velocity zone at an equivalent depth could correspond to a rising hot mantle under the most elevated part of the Central Tien Shan. This is also in line with the 40 mGal gravity low evidenced by Artemeviev et al. (1993) for the same area. From a 3-D seismic survey, Omuralieva et al. (2009) show that the seismic velocity structure under the Tien Shan at 20–50 km depth typically vary from high-velocity zones beneath the basins (including Issyk-Kul) and low-velocity zones beneath the mountain ranges. Using S-receiver functions, Kumar et al. (2005) further suggest that the topography is positively correlated with the depth of the lithosphere–asthenosphere boundary, which is locally deeper (~130 km) under North Tien Shan and shallower (~90 km) under the South Tien Shan highlands. Omuralieva et al. (2009) argue for the existence of small-scale convection cells in the mantle with upwelling beneath the mountain ranges

and downwelling beneath the large basins. At its southern margin, the Tarim platform is partly subducted under the Central Tien Shan range (Neil and Houseman, 1997; Yang and Liu, 2002), causing detachment folding of the Tien Shan–Tarim foreland (Scharer et al., 2004).

Unusually low heat flow values are reported by Vermeesch et al. (2004) for the Issyk-Kul basin, lower than expected for intermountain basins in a tectonic setting of crustal shortening and thickening, evidencing a relatively cold crust beneath the lake. Apart from a possible bias in measuring heat flow due to fluid circulation, two scenarios can indistinctly explain these observations: a uniform crustal thickening model or a lithospheric folding model, but the latter is favored by the geophysical constraints.

The strain rates derived from both GPS and seismological data show brittle deformation of the seismogenic crust dominated by N–S

shortening and accompanied by minor W–E extension (Tychkov et al., 2008). The 3D strain field corresponds to uniform horizontal contraction accompanied by intense vertical movements. Following the ideas of Bragin et al. (2001), they suggest that subsidence in the Issyk-kul basin is caused by a descending flow in the lower crust and mantle beneath the basin, compensated by mantle upwelling south of the lake. This mechanism is in line with what could be expected in the case of lithospheric folding (Burov et al., 1993; Cloetingh and Burov, 2011).

### 3. Early Cenozoic extension and late Cenozoic stress field change

The present-day stress field in Central Asia derived from the Harvard CMTS solutions (Fig. 1B) shows fan-shape  $S_{Hmax}$  trajectories with a NNW–SSW orientation (N170°E) in the Kyrgyz Tien Shan, N–S in eastern Tien Shan and Siberian Altai, NE–SE in East Sayan and Mongolian Altai and ENE–WSW in the Baikal rift. The focal mechanisms are dominantly thrust faulting in the entire Tien Shan, of mixed thrust and strike–slip faulting in the Altai and Sayan regions, and dominantly normal faulting in the Baikal rift.

Structural and geological fault–kinematic studies demonstrate that a regional change in stress regime occurred during the late Cenozoic, in the Baikal rift zone (Arjannikova et al., 2004; Delvaux et al., 1997; Sankov et al., 1997), Siberian Altai (Delvaux et al., 1995c), Kyrgyz Tien Shan (Delvaux et al., 2001) and northern Tibet (Xie et al., 1999).

Field investigations in the Kurai–Chuya, Zaisan and Issyk–Kul basins as will be detailed later show that the major compressional structures in Altai–Sayan and Tien Shan developed for a large part in the late Pliocene–early Pleistocene, during a period of major tectonic intensification. Since the middle Pleistocene, the tectonic deformation and basin evolution became less intense, defining a period of tectonic relaxation. This last period is still active today and is defined as the neotectonic period. Although much less well expressed, early Cenozoic N–S extension has been documented both the Chuya depression in Altai and Issyk–kul depression in the Tien Shan.

We compiled already published Cenozoic stress data for the Altai–Sayan and Tien Shan regions, from the Siberian Altai (Dehandschutter, 2001; Dehandschutter et al., 2002; Delvaux et al., 1995a, 1995c) and the Kazakhstan Altai (Glorie et al., 2012), and present new stress data acquired in the 1990's but not yet published (Table 1). For all these stress data, fault–kinematic analysis and paleostress inversion was done using the now classical methodology of brittle fault analysis described in Angelier (1994) and Dunne and Hancock (1994). The four parameters of the reduced stress tensor were determined on fault–slip data sets using the Win\_Tensor program (Delvaux, 2012), following the procedure described in Delvaux and Sperner (2003): the orientation of the three orthogonal principal stress axes  $\sigma_1$ ,  $\sigma_2$  and  $\sigma_3$  (with  $\sigma_1 \geq \sigma_2 \geq \sigma_3$ ) and the stress ratio  $R = (\sigma_2 - \sigma_3) / (\sigma_1 - \sigma_3)$  which expresses the magnitude of  $\sigma_2$  relative to  $\sigma_1$  and  $\sigma_3$ . For converting the results into stress trajectories, we computed the horizontal principal compressional stress  $S_{Hmax}$  following Lund and Townend (2007) and determined the stress regime index  $R'$  as in Delvaux and Sperner (2003). The latter forms a continuous scale from 0 (radial extension) to 3 (constriction) and ranges from 0 to 1 for normal faulting regimes, from 1 to 2 for strike–slip regimes and from 2 to 3 for thrust faulting regimes.

In function of structural and stratigraphic relations, the paleostress results have been attributed to the basin initiation stage (Eocene–Miocene; Table 1a), the tectonic intensification stage (late Pliocene–early Pleistocene; Fig. 4 A–B; Table 1b) or the neotectonic relaxation stage (middle Pleistocene–Holocene; Table 1c). On rose diagrams (Fig. 5), the  $S_{Hmax}$  show a general trend defined by a major population but often also secondary trends. These major populations have been separated from the minor ones using the dynamic separation algorithm of Huang and Charlesworth (1989).

No significant differences can be noted between the  $S_{Hmax}$  orientations associated with the Harvard CMT focal mechanisms (Fig. 1B)

and the ones corresponding to the middle Pleistocene–Holocene paleostress stage. Instead, significant clockwise rotation in  $S_{Hmax}$  orientation is observed between the late Pliocene–early Pleistocene and the middle Pleistocene–Holocene stress stages: 27° in Altai–Sayan (from N180 to 207°E; Fig. 5A) and 56° in the Tien Shan (from N130 to 186°E; Fig. 5B). Conversely, the average stress regime becomes slightly more strike–slip in Altai–Sayan (average  $R'$  from 2.1 to 1.9), although it remains similar in Tien Shan ( $R' = 2.0$ ).

The late Cenozoic stress change implies that the major structures were generated by a different stress field than the currently acting one. In consequence, some structures that have been active during late Neogene–early Pleistocene are now inactive and others are reactivated but with a different kinematics. This change occurred between early- and middle Pleistocene (~1 Ma ago) and marks the onset of the neotectonic period. The causes for this stress change is known but it seems to have affected a large part of Central Asia.

The onset of compressional stresses in the late Pliocene does not seem to be related to any known change in plate kinematics (Le Pichon et al., 1992) that could modify the forces applied at the plate boundaries, but can be tentatively explained by the uplift of the Tibet Plateau. Using finite element modelling, Vergnolle et al. (2007) showed that the present-day deformation in the Himalayas, Tibet, Tien Shan and Altai where N–S shortening prevails can be explained by the buoyancy forces generated by integrating the gravitational potential energy gradients (GPE) in Asia, the forces provided by the convergence of oceanic plates towards Eurasia and oceanic subduction coupling. They concluded that buoyancy forces alone or forces related to the India–Eurasia alone are insufficient to explain the present-day deformation and demonstrated that both contribute in a significant and comparable way. As the GPE distribution in Asia is strongly influenced by the Tibet plateau, we propose that the observed stress change could be related to the dynamics of the Tibet plateau uplift. As shown by Vergnolle et al. (2007) uplift of the wide Tibet Plateau generates buoyancy stresses that could modify the intraplate stress that prevailed during the Oligocene–Miocene in Central Asia and cause the onset of the tectonic intensification stage. As an evidence, at the foot of the Kunlun Mountains, Zheng et al. (2000) noted a marked change in depositional facies accompanied by an increase in sediment rate and sediment coarsening in the Pliocene (~3.5 Ma) that they relate to the main uplift of the northern Tibet Plateau.

### 4. Fourier transform analysis of topographic profiles

As shown by Burov et al. (1993), Burov and Molnar (1998), Burov and Cloetingh (1997) and Cloetingh and Burov (2011), crustal folding can be evidenced from surface topography, morphotectonics and free air gravity, while the lithospheric mantle folding is reflected by the Moho deflection and can be traced from Bouguer gravity anomalies. Mantle folding can also have topographic signature, especially when it is coupled with crustal folding (e.g. Sokoutis et al., 2005). Here, we only used the topographic profiles as the tectonic morphology is sufficiently well preserved to image the lithospheric folding. The dominant topographic wavelengths were obtained by Fourier transform analysis.

A series of topographic profiles have been extracted from the Etopo-30 topographic database. These were constructed in the average direction of  $S_{Hmax}$  for the late Pliocene–early Quaternary stage of tectonic intensification as lithospheric folds largely developed during this period. The coordinates of the extracted data points have been converted into UTM projection and the distance along the profiles expressed in kilometers. Because the original profile data were not equidistantly spaced, an interpolation scheme was applied to create elevation profiles with equidistant x-positions, using a spacing of 1 km.

Optimizing the Fourier transform requires the number of input samples to be a power of 2 (e.g. 512, 1024). Instead of extrapolating the profiles up to the nearest power of 2 value by filling up the elevations with zeros, the Fourier scripts have been adapted for profiles independent of

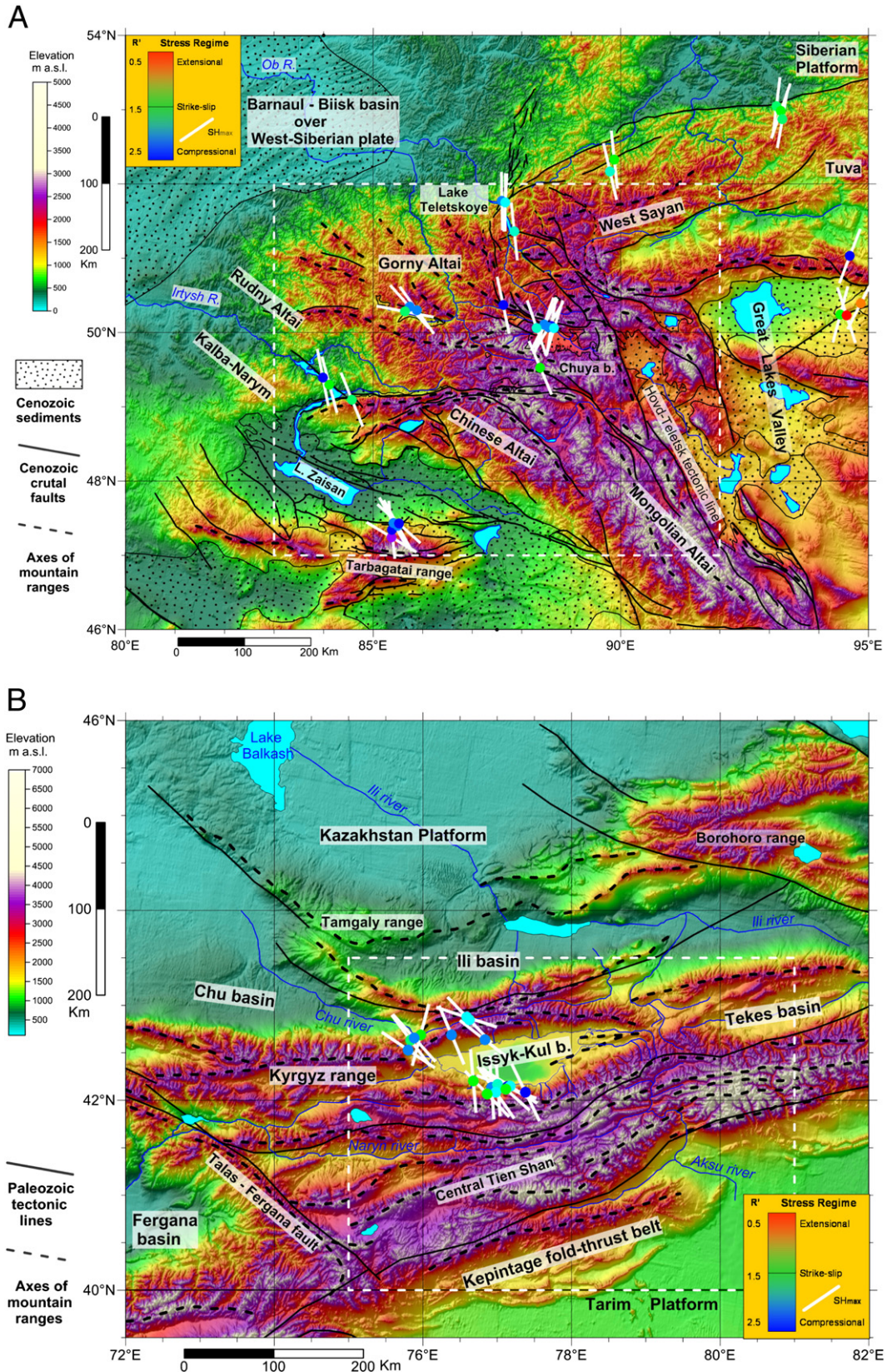


**Fig. 4.** Morphostructural maps for Altai–Sayan (A) and Tien Shan (B) with stress data for the late Pliocene–early Pleistocene. Dashed: location of Fig. 8(a,b). Black dotted lines: axes of mountain ranges; solid lines: Cenozoic crustal faults for Altai–Sayan and Paleozoic tectonic lines for Tien Shan.  $S_{Hmax}$  orientations as white bars and colored filled circle for stress regime index  $R'$ .

their length, so that the computed spectra are based on the original length of the profiles. The differences between the two methods are minimal, though not affecting the interpretations.

The wavelength spectra of all profile lines clearly include several dominant wavelengths (Fig. 6, Table 2a). This is what could be expected for a folded stratified lithosphere, with the upper crust decoupled from

the lithospheric mantle (Burov et al., 1993). However, distinctions between separate dominant wavelengths are not always clear, as the relation between the dominant wavelengths of a series of neighboring lines is not always obvious. As a common characteristic, all lines have a short dominant wavelength component between roughly 40 and 60 km.

For the Altai–Sayan, the short wavelength component is decreasing eastwards from 60–70 km (AS1) to 30–40 km (AS5). The intermediate wavelength displays the same trend, decreasing eastwards from 100–120 km (AS1) to 75–90 km (AS5). The long wavelength (200–300 km) is better expressed in the extreme east (AS1) and fades westwards (AS3) after which it is no longer expressed. Instead, additional intermediate wavelengths appear for AS3 (ca 160 km), AS4 (150–180 km) and AS5 (110–135 km).

For the Tien Shan, all lines show long wavelength components, increasing eastwards from 150–200 km (TS1–TS4) to 250–350 km (TS5–TS6). Except for TS1, all the lines show also intermediate wavelength, increasing eastwards from 110–140 km (TS2) to 140–180 km (TS6). Wavelengths below 100 km are less well expressed and more variable. A 70–80 km wavelength is clearly distinguishable in lines TS1–TS3 and TS6, but appears combined with shorter wavelength in

TS4 and TS5. Short (ca 40 km) wavelengths are present on TS1 and TS2, but are absent on TS3 and TS6 and combined with intermediate ones on TS4 and TS5.

These results show that the wavelength spectra of Altai–Sayan and Tien Shan are comparable to some degree. A striking characteristic is their lateral variations. They all have short wavelength (40–60 km), but this is better expressed in Altai–Sayan. The long wavelength reaches 200–300 km in the western half of Altai–Sayan and are no longer expressed in the eastern part (Kurai and Chuya area). In Tien Shan, conversely, the long wavelength (200–350 km) is well expressed for all lines, but not significantly different from the Altai–Sayan ones.

The relation between folding wavelength and thermotectonic age can be expressed in a wavelength versus thermotectonic age plot (Fig. 7), in which the paths relative to the different folding type has been defined on the basis of experimental and observational data (Burov et al., 1993; Cloetingh and Burov, 2011). First-order (longer) wavelengths which reflect lithospheric mantle folding and whole lithosphere folding are dependent on the thermotectonic age, especially when <600 Ma, while second-order (shorter) wavelength which reflect crustal folding are almost independent. In this reference diagram, the

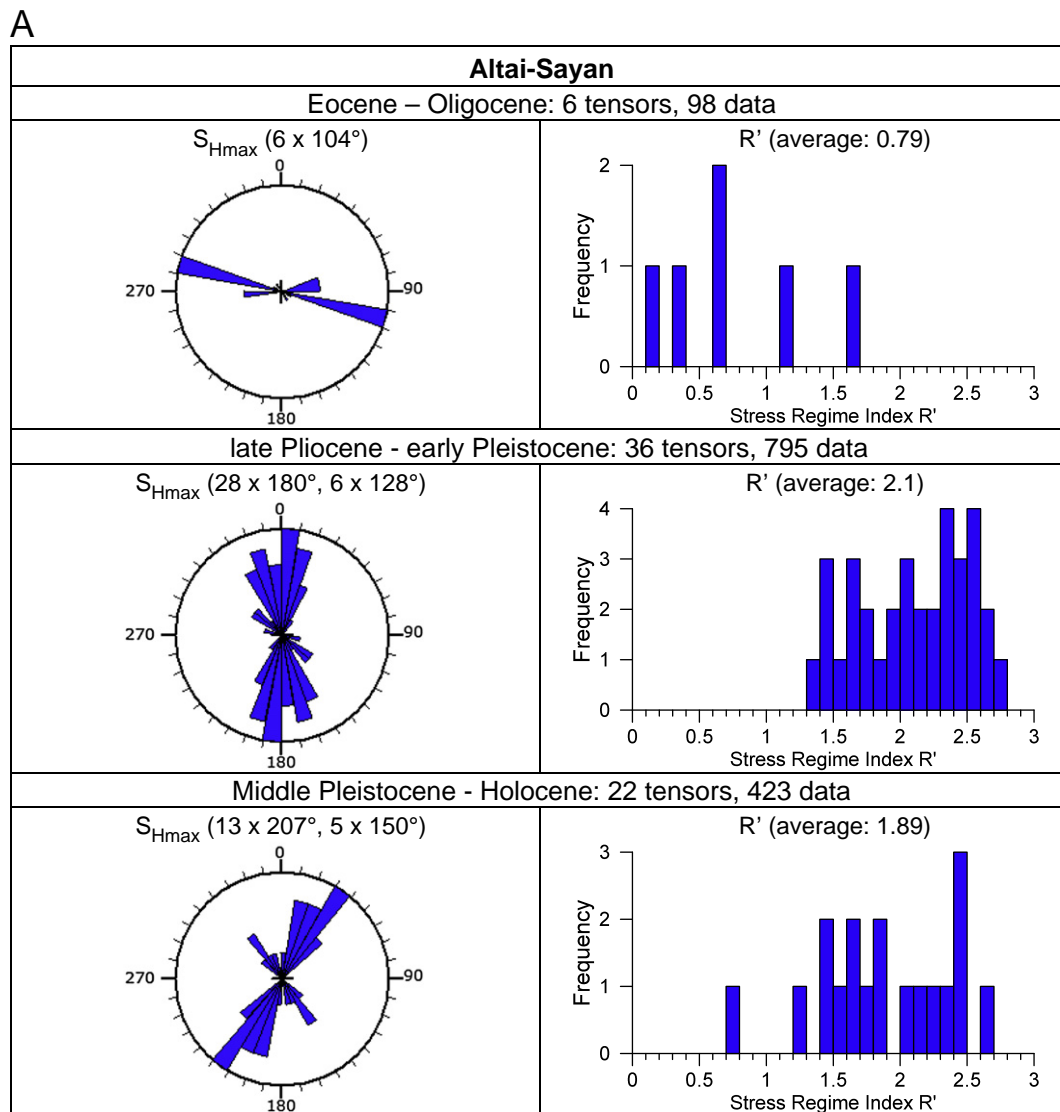


**Fig. 5.** Stress inversion results for Altai–Sayan (top) and Tien-Shan (bottom), for the late Pliocene–early Pleistocene tectonic intensification stage and the middle Pleistocene–Holocene neotectonic relaxation stage. Left: Rose diagrams for azimuth of  $S_{Hmax}$ . The average orientations of  $S_{Hmax}$  are presented for the dominant and min of populations together with their number of data. Right: histograms for stress regime index  $R'$ .

**B**

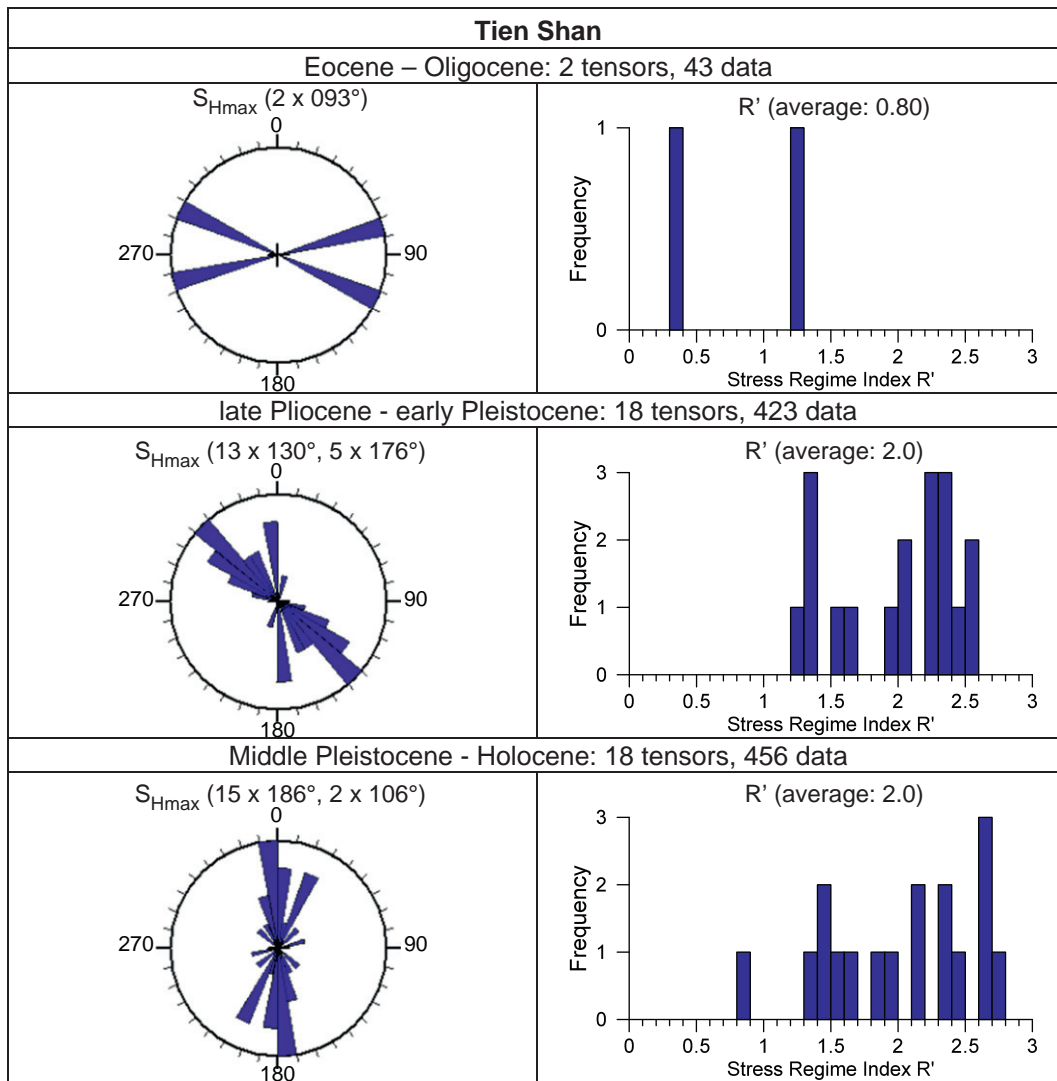


Fig. 5 (continued).

spectral data obtained for Altai–Sayan and Tien Shan plot in the paths of decoupled lithospheric mantle and crustal folding. For both areas, the lithosphere is heterogenous with different thermotectonic age along strike (Altai–Sayan) or across strike (Tien Shan). Because strain is expected to localize in weaker regions, the most recent thermotectonic age was used. We further consider as first-order wavelengths, those above 220 km for Altai–Sayan and 199 km for Tien Shan, and as second-order wavelengths, those less than 100 km (Tables 2a and 2b).

**5. Tectonic morphology**

The surface expression of lithospheric deformation (folding and faulting) in Central Asia is well documented by the tectonic morphology thanks to the youthfulness of the relief. It is investigated here on the basis of morphotectonic maps displayed over altitude color-coded and artificially shaded SRTM-3 digital topographic data (Fig. 8A–B). In both regions, the late Mesozoic–early Cenozoic planation surface is taken as reference for defining topographic undulations and fault-related displacements. This surface has been largely affected by erosion in the mountain ranges and is concealed under Cenozoic deposits in the sedimentary basins. But it can still be seen as flat top summits and at the knick points along the range-basin transition and has been

imaged by geophysical investigation and drilling in the basins (Fig. 9). We document here the large-scale upper crustal structures for the entire belts in order to evidence the general relations between faulting, folding, thermotectonic age and basement heterogeneities.

**5.1. Altai–Sayan**

The Altai belt in Siberia (Fig. 8A) has a general NW–SE trend. It has a fan shape to the northwest (Gorny Altai and Rudny Altai) and is narrowing progressively to the southeast while the relief is becoming more rugged (Mongolian Altai). It is separated by the NNW–SSE Hovd-Teletsk tectonic line from the West Sayan massif (Tuva region of Siberia) and the Great Lakes Valley of Mongolia. This tectonic line corresponds on its northern portion to the 50 km-long Teletsk Gaben linked to the Shapshal fault (Dehandschutter et al., 2002; Delvaux et al., 1995a; Dergunov, 1972), itself connected southwards to the Hovd fault in Mongolia. West of this line, the Altai belt is internally structured as a series of thrusts and strike-slip faults, defining longitudinal ridges and controlling the morphology (Bayasgalan et al., 1999; Cunningham et al., 1996; Schlupp, 1996). The crustal segments between faults of opposing vergence are either bent downwards, forming sedimentary basins as for the Kurai and Uymon depressions, or upwards, as in the

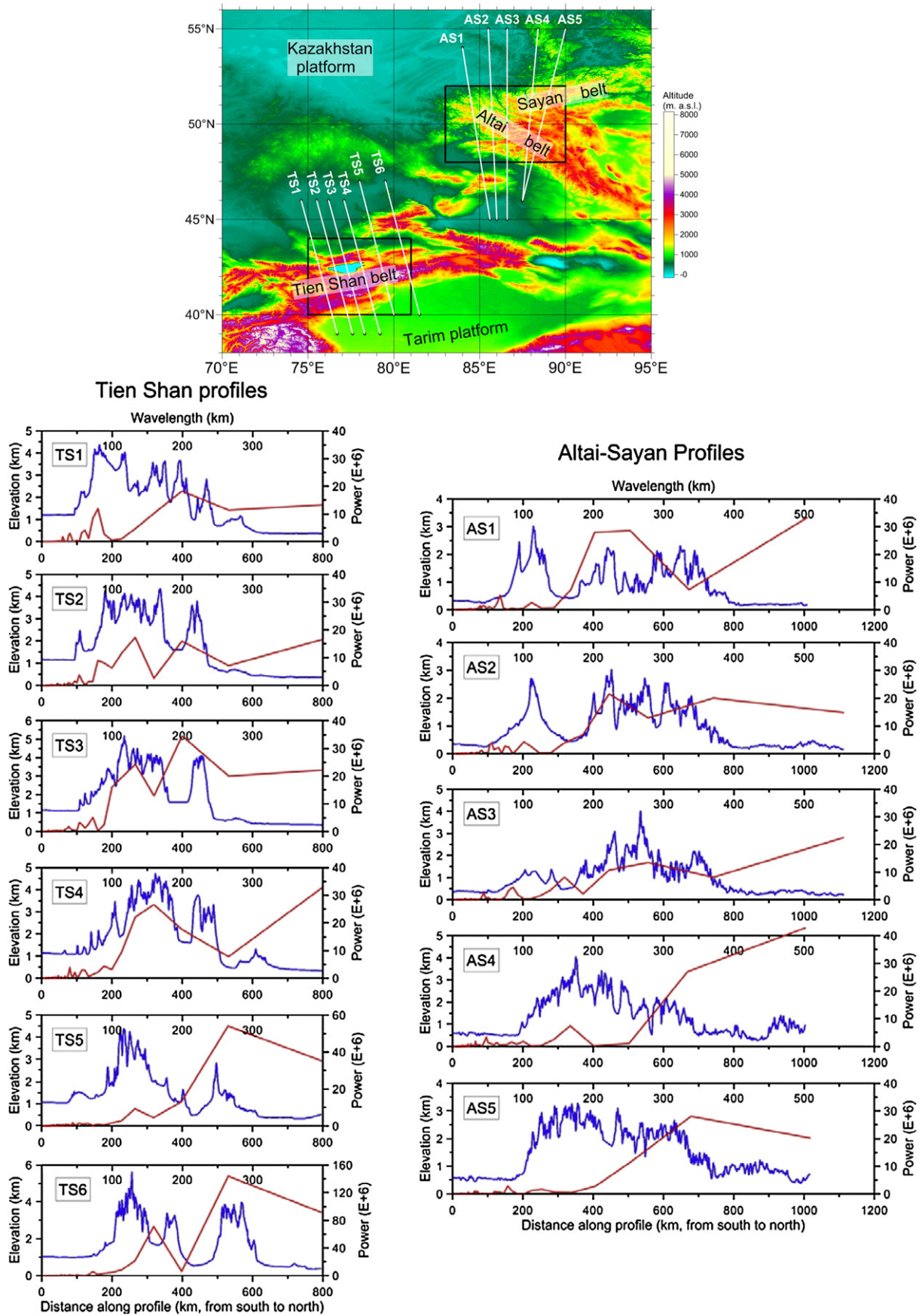


Fig. 6. Topographic profiles (blue lines) with Fourier transform spectral analysis (red lines). Top panel shows location of profiles. Left column: Tien Shan profiles (TS1–6); right column: Altai–Sayan profiles (AS1–5).

**Table 2a**  
Fourier transform wavelength spectra of topographic profiles. W: wavelength (km), Power: spectral power ( $\times 10^6$ ).

Profile description					Wavelength spectra												
Profile		Begin		End		Short				Intermediate				Long			
Code	Name	Long	Lat	Long	Lat	W (km)	Power (E+6)	W (km)	Power (E+6)	W (km)	Power (E+6)	W (km)	Power (E+6)	W (km)	Power (E+6)	W (km)	Power (E+6)
Altai–Sayan																	
AS1	Zaisan–Rudny Altai	85.6	45	84	54	67	5.26					112	2.56	201	27.94	252	28.64
AS2	Markakul–Uymon	86	45	85.5	55	53	3.47			74.13	2.75	101	4.27			222	21.62
AS3	Belucha	86.6	45	86.6	55	44	2.60			86	4.59			159	8.19	278	13.47
AS4	Kurai	87.5	46	88.4	55	47	3.44			83	1.54	100	1.75	167	7.43		
AS5	Ukok–Chuya	87.5	46	90	55	35	9.75	59	8.70	78	2.91	127	1.25				
Tien Shan																	
TS1	Kochkor	76.7	39	74.6	46	39	2.92	61	4.06	79	1.19			199	18.30		
TS2	Issyk Kul West	77.6	39	75.5	46	38	1.08	53	3.74	80	8.94	133	1.73	199	15.93		
TS3	Issyk Kul Center	78.3	39	76.2	46	38	1.86	53	3.21	72	5.10	133	24.32	200	34.54		
TS4	Issyk Kul East	79.2	39	77.1	46	40	3.91	59	3.00	88	4.39	159	26.64				
TS5	Tyup	80	40	78	47	44	1.84	53	1.53	79	0.74	133	9.30	265	54.13		
TS6	Pobedy–Tekes	81.5	40	79.5	47	49	1.31			72	5.83	159	71.13	265	143.90		

Ukok plateau and the Katun range which is culminating at 4506 m (Belukha peak). Between faults of similar vergence, crustal segments deform as half-ramps with pronounced tilting, as in the Chuya and Zaisan depressions.

On the western side of the Altai range, sections AS1–AS3 (Fig. 9) transect successively the Tarbagatai range, the tilted floor of the Zaisan depression, the South Altai asymmetric range with the faulted Lake Markakul step, the Bukhtarma narrow valley, the Katun broad ridge, the Uymon intramontane depression and the Terektin and Cemin ranges of decreasing altitude. The South Altai range is separated from the Bukhtarma valley by the South–Altai thrust system in a 2000 meter high topographic step (Fig. 10, profile A–A). The broad Katun range is not fault-controlled, but the northern boundary of the Uymon depression is marked by a low-angle thrust fault. The other undulations in Gorny Altai are not clearly associated to faulting.

Further to east, sections AS4–AS5 (Fig. 9) are running from the Chinese Altai trough the Kurai–Chuya depression and the West Sayan massif. The topography on the southern flank of the South Altai range

rises northwards gradually and stepwise, to 4374 m high at the triple point between Mongolia, China and Siberia (Nairamdal range). It rapidly lowers in association to reverse faulting towards the Bertek depression (2600 m high). The Ukok plateau which hosts important archeological sites in permafrost is formed by the remnants of a low anticline ridge. It is separated from the South Chuya range by the Argut glacial valley, apparently without reverse faulting as sometimes drawn. The profile continues by the Kurai and Chuya depressions, the Kurai ridge, the Bashkaus valley, the Shapshal valley and ends by the West Sayan broad uplift (Fig. 10, profile B–B').

5.2. Kyrgyz Tien Shan

The Tien Shan belt in NE Kyrgyzstan and S Kazakhstan (Fig. 8B) is trending ENE to E, with the Issyk-Kul and Tecs basins forming large almond-shaped intramontane depressions. S–N sections (TS1–TS6) trough the Kyrgyz Tien Shan, from the Tarim platform (~1050 m a.s.l.) to the Kazakhstan platform (~350 m a.s.l.), are displayed on Fig. 9. In the Kashi foreland against the Tarim platform, the Kepintage fold-and-thrust belt develops with a southwards thrusting direction (Heermance et al., 2008; Scharer et al., 2004). The relief rises stepwise towards the Karateke range, which is separated from the Kokshal range by the Tauchkandaria valley. It reaches the high-altitude Central Ten Shan region (3500–4500 m) and is drained longitudinally by the Naryn and Aksu rivers. After the 5125 m high Ak-Siyrak–Kalyu range which forms a large topographic undulation, the Kumtor plateau develops as a slightly south-westerly tilted portions of the former planation surface, between 3800 and 4300 m high (Fig. 11). The Terskey range (up to 5216 m) forms the transition between the Kumtor plateau and the Issyk-Kul depression. The latter contains up to 3500 m of late Cenozoic sediments and is partly occupied by Lake Issyk-Kul (1600 m high, 670 m deep). The basin is closed on its northern side by the coupled Kungey (4980 m) and Zaili (4650–4760 m) ranges separated by the Chon-Kemin–Chilik valley and related transpressional fault, forming a positive flower structure. The Zaili range is partly thrust

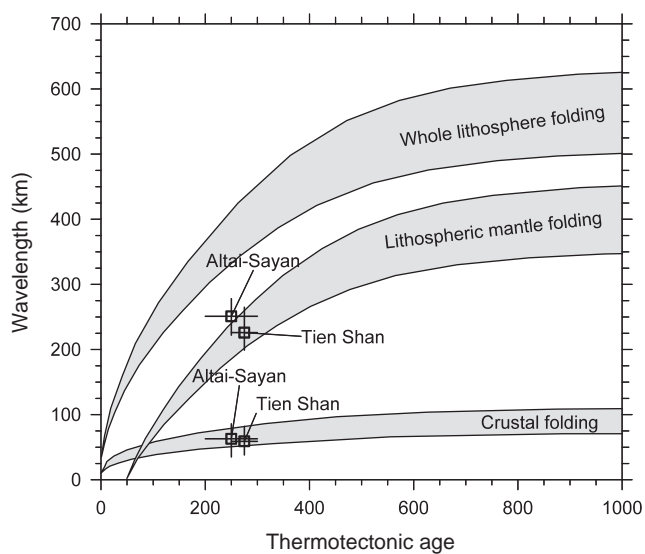


**Fig. 7.** Relationship between wavelengths of lithospheric folding and thermo-tectonic age of lithosphere. The gray zones correspond to the paths of theoretical folding wavelengths for the upper crust, mantle and coupled whole mantle folding (after Cloetingh et al., 1999). Black squares show short and long wavelengths from spectral analysis of topographic profiles in Altai–Sayan and Tien Shan (Table 2b).

**Table 2b**  
Average and range of values for the thermotectonic age and folding wavelength in Altai–Sayan and Tien Shan (based on Table 2a.)

Region	Thermotectonic age (Ma)			Short–intermediate wavelength			Long wavelength		
	Min	Average	Max	Min	Average	Max	Min	Average	Max
Altai–Sayan	200	250	300	35	63	86	222	251	278
Tien Shan	250	275	300	38	59	82	199	226	265

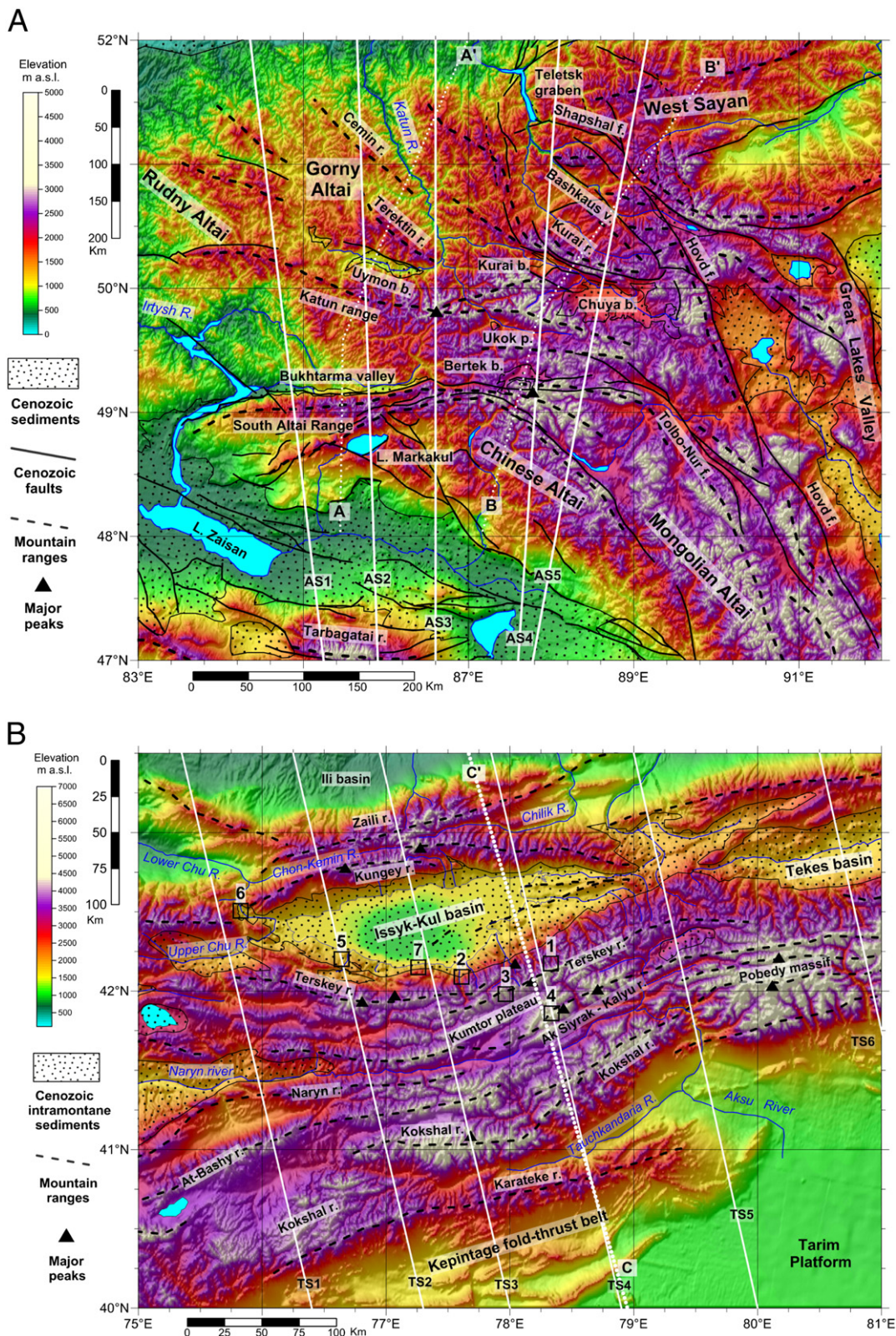


**Fig. 8.** Topography for (A) Siberian Altai–Sayan and (B) Kyrgyz Tien Shan with location of major Cenozoic faults and basins. Location in Fig. 4. Names of ranges (r.), lakes (L), valleys (v.) and basins (b.). Bathymetry of Lake Issyk-Kul digitized from 1:100,000 bathymetric map. Detailed sites around Lake Issyk-Kul are shown by an empty square: 1 (frontal view of the Terskey range, Fig. 11A), 2 (Tosor valley unconformity, Fig. 11B), 3 (Kumtor plateau, Fig. 11C), 4 (Ak-Shiyrak range, Fig. 11D), 5 (Bokombaievskoye fault-propagation fold, Fig. 12), 6 (Boom pop-down syncline, Fig. 13) and 7 (Kadji-say upward extrusion, Fig. 14). Dotted lines show location of interpreted profiles displayed in Fig. 10.

over the Ili foreland basin against the Kazakhstan platform. In the latter, low-amplitude but long wavelength undulations can still be observed, with the Tamgaly range in continuation of the Borohoro range and further north, the Balkhash closed and shallow depression.

**6. Intramontane basin structure and evolution**

The Kurai-Chuya basin in the Gorny Altai republic of Russia, the Zaisan basin in NE Kazakhstan, and the Issyk-kul basin in the Kyrgyz

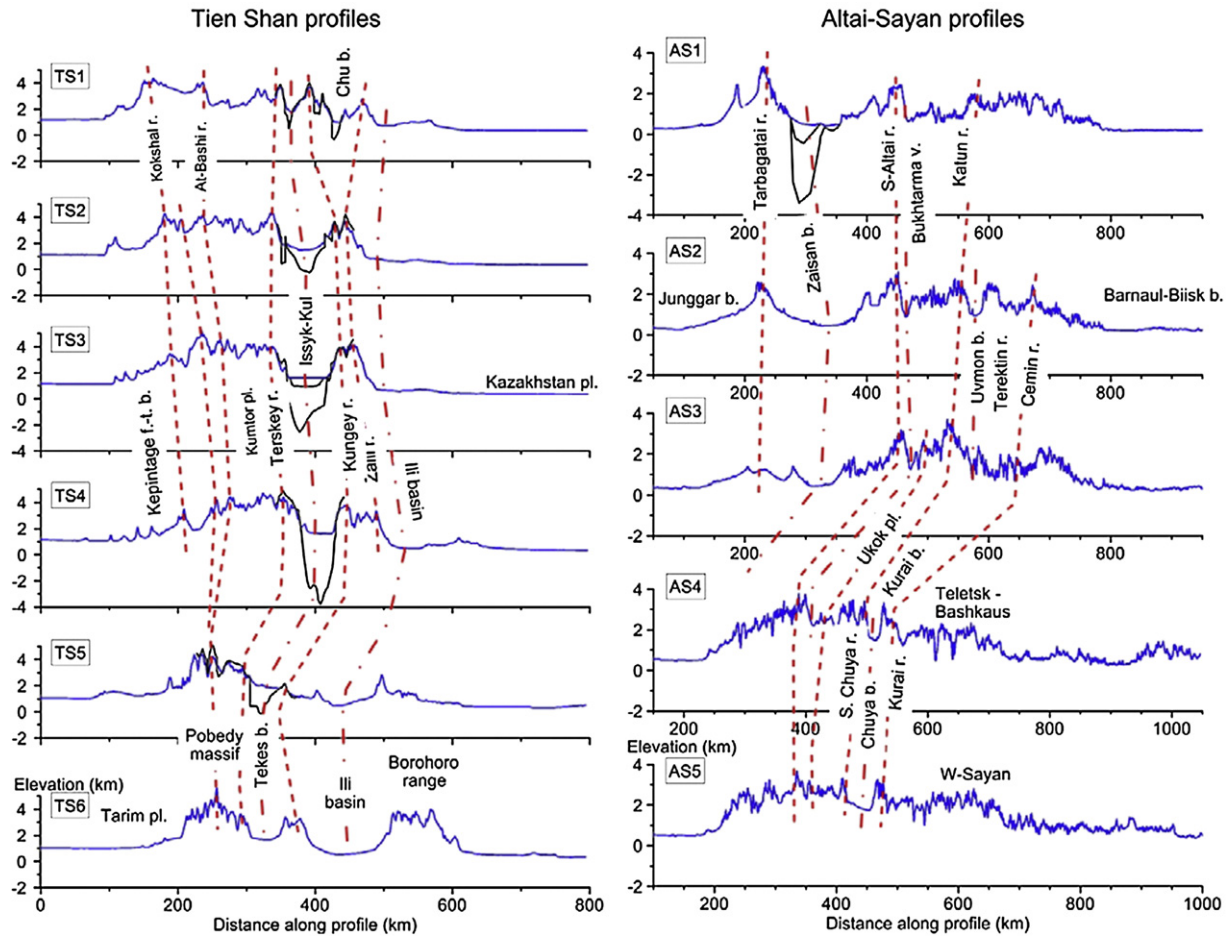


Fig. 9. Topographic profiles extracted from the Etopo30 digital topographic database across the Tien Shan (left column, profiles TS1–6) and from the SRTM-3 database (90 meter resolution) across the Altai belt (right column, profiles AS1–5).

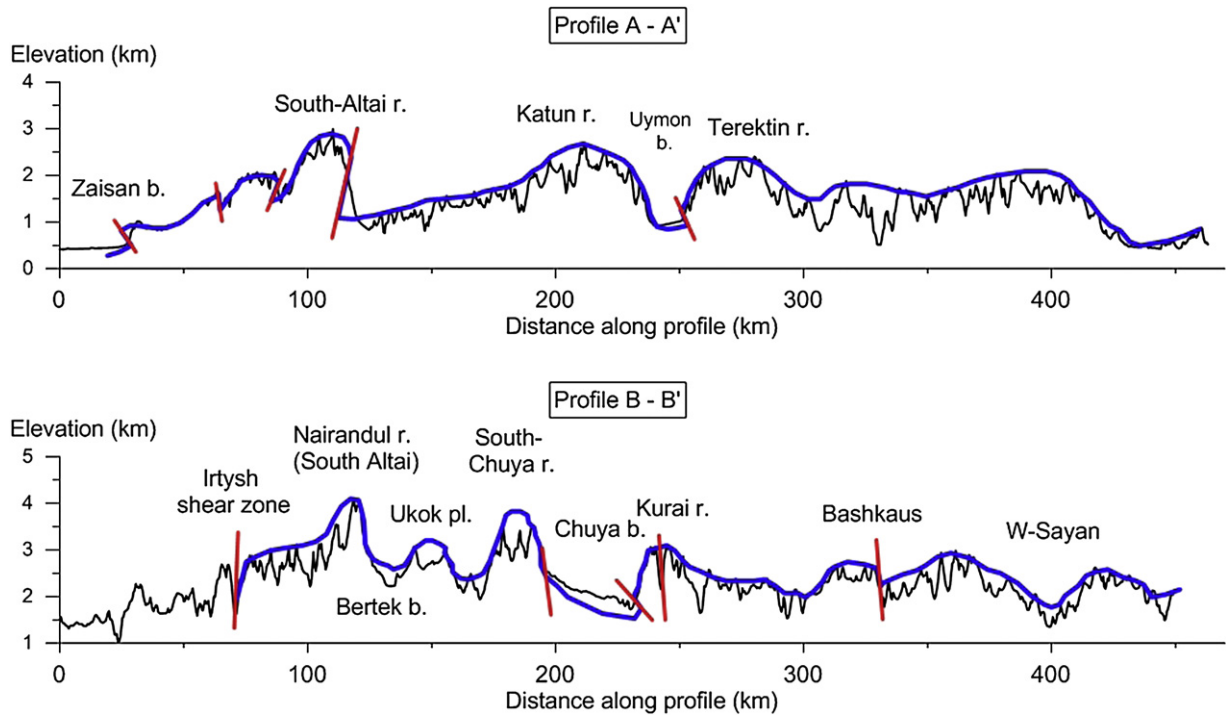


Fig. 10. Interpreted Altai-Sayan topographic sections with deformed late Cretaceous–Paleogene erosion surface on top of pre-Cenozoic basement (Fig. 8A, dotted lines).



**Fig. 11.** Evidence for syn-sedimentary extension (A) in the Chuya basin (Taldy-Dyurgun brown coal deposit in the Oligocene Koch-Agach formation) and (B) in the northwest margin of the Issyk-Kul basin at Toru-Aigir (in the Eocene Kyzylgir formation).

Tien Shan are typical intraplate basins developing on a folding lithosphere. They have been initiated in an extensional context, before the late Tertiary tectonic inversion. Their investigation presents a particular interest as they have recorded in their stratigraphy, morphology and tectonic structures the processes of basin compressional inversion in a folding lithosphere.

### 6.1. Kurai and Chuya basins in the Siberian Altai

#### 6.1.1. Basin morphology

The Kurai and Chuya depressions are entirely surrounded by mountain ranges and drained by the Chuya River (Figs. 8a, 10). They have respective dimensions of  $20 \times 30$  and  $60 \times 90$  km and the average elevation of their floor is respectively at 1500–1600 and 1750–2000 m. Taking into account that the two depressions probably initiated as a single one (Delvaux et al., 1995c), the total length of the initial basin amounts 130 km. Both the depressions are bordered on their northern side by the Kurai range (3412 m). The Kurai depression is limited to the south by the North-Chuya range (4174 m). This range extends to the east

and north-east by the Chagan–Uzun uplift (2900 m) which separates the Kurai and Chuya depressions. The Chuya depression is asymmetric, rising progressively southwards towards the South-Chuya range (3936 m). It contains up to 1200 m of Cenozoic sediments (drilled over 671 m) and the Kurai depression, almost 1000 m (Buslov et al., 1999; Deviatkin, 1965; Luzgin and Ruzanov, 1992).

#### 6.1.2. Tectonostratigraphic evolution

The Kurai and Chuya depressions develop at the margin of the Vendian–Devonian Altai–Mongolia and the Vendian–Cambrian Gorny–Altai terranes, along the Charysh–Terekta shear zone. Their tectonostratigraphic evolution since the late Mesozoic has been reviewed by Delvaux et al. (1995c), Buslov et al. (1999), Thomas et al. (2002) and De Grave et al. (2007b). In the Santonian–Campanian, a short marine transgression over the late Cretaceous planation surface shows that this region was at a low altitude before the Tertiary (Buslov et al., 1999). The former unique basin started to develop in the late Eocene–early Oligocene in a graben-like structure limited to the northern half of the present depression. Sedimentation occurred first by reworking and

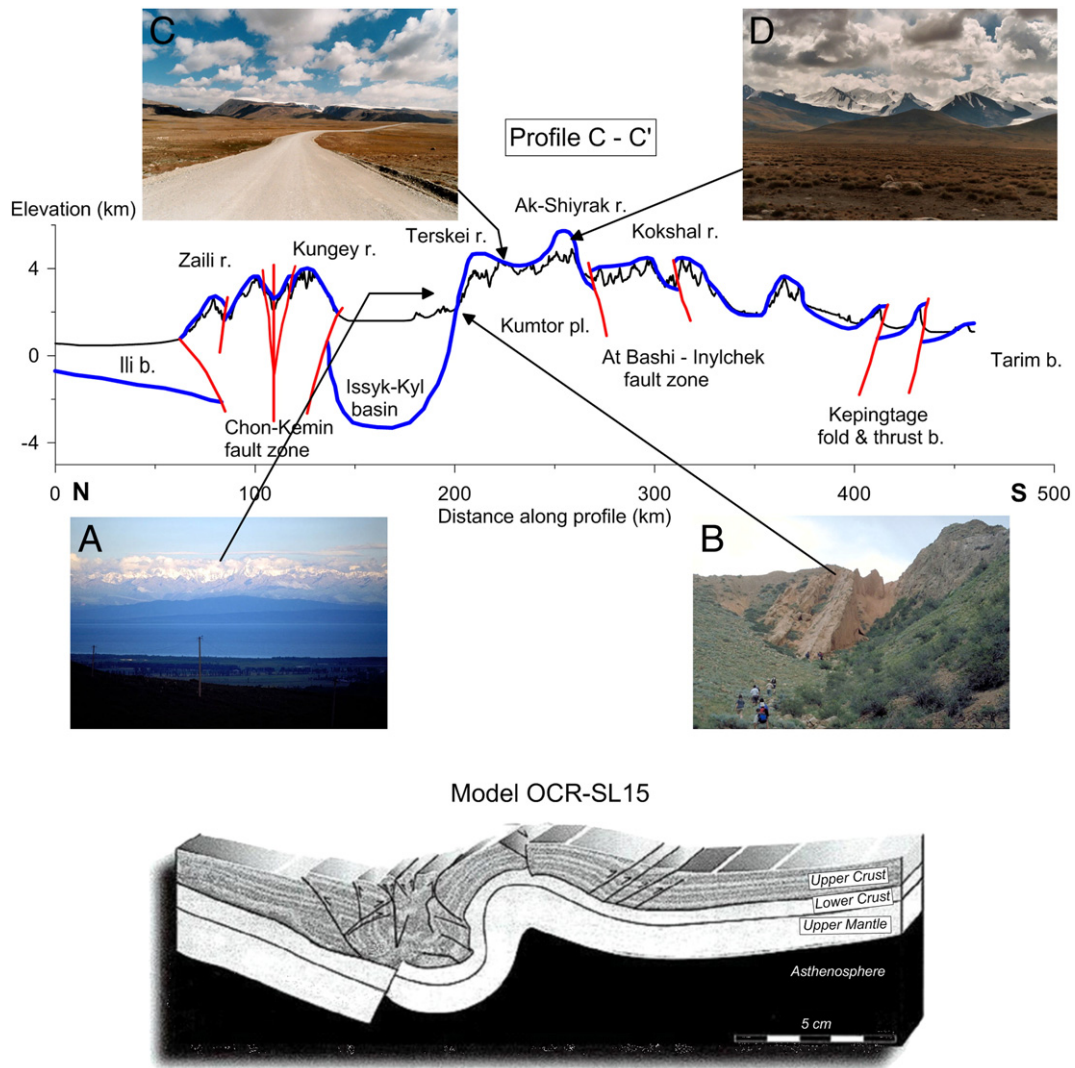


**Fig. 12.** Transition from Lake Issyk-Kyl to Kumtor plateau along profile C–C' (marked as dotted lines in Fig. 8B). Picture A: frontal view of the southern margin of Issyk-Kul depression (site 1 in Fig. 8b), B: tilted unconformity along the Tosor River (site 2 in Fig. 8B), C: late Cretaceous–Paleogene peneplain preserved as flat top slightly tilted to the south under an ice cover (site 3 in Fig. 8B), D: Ak-Shiyrak range forming a well-preserved anticlinal undulation (site 4 in Fig. 8B). Bottom: comparison with the analogue model OCR-SL15 of Sokoutis et al. (2005).

redeposition of materials from the late Cretaceous–Paleocene weathering crust, in a subtropical environment (*Karachum* red continental molasses grading to red/white clay deposits). Facies relationships and the presence of syndimentary tectonic structures indicate that deposition of the *Karachum* was controlled by syndimentary normal faulting (Fig. 11).

In Miocene–early Pliocene, the depositional environment became progressively more lacustrine, with well-developed proximal and lacustrine facies. The early–middle Miocene *Kosh-Agash* formation is composed of shallow lacustrine coal-bearing clays and the early Miocene *Tueryk* formation, of deeper lacustrine carbonate clays. Limited evidence for syndimentary extension in the *Kosh-Agash* formation is found in the Taldy-Durgum coal deposit by a where a syn-sedimentary listric normal fault (Fig. 11). In late Miocene–early Pliocene, the lake was progressively filled by mudstone with an abundant and well-dated fauna of freshwater mollusks, ostracods, fish, mammals and plants that reached a high degree of endemism (*Kyzylgir* formation; Zykin and Kazansky, 1995).

At the end of the early Pliocene, the lake was completely filled and a stromatolith layer developed over the inundated flat bottom of the depression, indifferently over the sediment and the basement rocks. The lacustrine stage was interrupted in late Pliocene, about 3.5 Ma

ago, by a vigorous transpressional inversion (Buslov et al., 1999; Delvaux et al., 1995c). Coarse sands and gravels of the *Becken* formation were first deposited over the stromatolitic surface. They were followed by early Pleistocene molassic sediments of the *Terek* and *Bashkaus* formations, as the Kurai range was rising and partly trusted over the northern part of the Kurai and Chuya sub-basins (Fig. 10). Development of inversion structures and related molassic sedimentation reached a maximum intensity in the early Pleistocene. Deformation relaxed in the middle Pleistocene and the deposition area expanded towards the south, further than the limits of the initial graben. Inversion structures probably also affected the southern part of the Oligocene–Miocene depression, but these are concealed under the Quaternary deposits (Buslov et al., 1999). This episode of basin inversion, which started at ~3.5 Ma and lasted until ~1 Ma, represents a period of intense tectonic shortening. It was apparently preceded by a short period of slow shortening that caused limited relief formation, erosion and the progressive infill of the Chuya paleolake. Since middle Pleistocene, successive glaciations caused the development of glacial moraines that blocked intermittently the Chuya river valley and formed a large lake in the Kurai and Chuya depressions. The glacial processes caused intense erosion in the ranges with the development of U-shaped glacial

valleys and glacial fluvio-lacustrine sedimentation in the basins. Deformation continued up to the Present-day, as shown by the 2003 Chuya earthquake (Nissen et al., 2007).

### 6.1.3. Basin and range-basin margins structure

As reviewed above, the Kurai–Chuya basin system originates as a graben and was inverted as a ramp of half-ramp during the late Pliocene–early Pleistocene. The Kurai sub-basin remained symmetrical while the Chuya sub-basin gained its asymmetry during the transpressional inversion.

The structure of the Kurai range at the northern margin of the Kurai–Chuya basin is dominated by the Kurai transpressional fault, which itself reactivates the late Paleozoic Kurai shear zone. It is curved in plan view and appears as a transpressional positive flower structure with a subvertical master fault in the center of the range and a southward verging thrust system on the basin side. North of the Chuya depression, the boundary thrusts are well individualized from the master fault (Figs. 8a, 10). Westwards, the marginal thrusts merge with it, forming a NE-dipping reverse fault system at the northern margin of the Kurai depression (Bondarenko, 1976).

The southern margin of the Kurai sub-basin is largely concealed under thick glacial deposits and limited abruptly by the North Chuya range. In contrast, the floor of the Chuya sub-basin rises progressively southwards. The transition of the Chuya basin with the South Chuya range corresponds to a morphological break, possibly controlled by a fault line concealed under the late Quaternary glacial sediments (Delvaux et al., 1995c). The entire southern margin of both the Kurai and Chuya depressions ruptured during the 2003 Siberian Altai earthquake sequence. The largest shock (*M*<sub>w</sub> 7.2) generated surface breaks over a total length of about 60 km, aligned along a fault striking 295°E with was activated by right-lateral strike–slip movement with a slight reverse component (Agatova et al., 2004; Nissen et al., 2007; Rogozhin et al., 2003). On the south-western side of the Kurai depression, after-shock distribution shows that the fault plane dips steeply towards the SW under the North Chuya range, confirming the opinion that the southern margin of the Kurai basin is fault-controlled and of ramp-type (Novikov et al., 2008). In contrast, on the south-western side of the Chuya depression, the fault plane dips 55–85° NE under the basin center, causing uplift of the basin floor relative to the adjacent mountain range. This is opposite to the sense that would be expected if this side of the basin was characterized by a ramp system. SAR interferometry patterns (Nissen et al., 2007) confirm that the dominant mechanism is dextral strike–slip along a NW–SE steep fault dipping NE.

Integrating a longer period of measurement than in Calais et al. (2003), Goldin et al. (2005) found a GPS-derived convergence rate of 8–9 mm/yr within a distance of 100 km between the Ukok plateau and the Kurai range.

The topographic undulations south of the Chuya depressions are described above together with sections AS4–AS5 (Fig. 9). More details are provided in profile B–B' (Fig. 10).

## 6.2. Zaisan depression

### 6.2.1. Basin morphology

The Zaisan depression is ±200 km long, 25–30 km wide with its floor at 403 m a.s.l. and hosting Lake Zaisan with a maximum depth of 15 m (Fig. 6). Seismic profiling and drilling evidenced that the central part of the basin contains about up to 2000 m of (mostly) Permian to Mesozoic series up to 800 m of Paleogene profile B–B' sediments and a similar thickness of Neogen. Relicts of the late Cretaceous–Paleogene planation surface are preserved on the tilted flanks the basin, as kaolin bearing weathering crust and Paleogene sand with white quartz pebbles, up to 3500–3600 m high north of the basin and up to 3800 m high south of it (Thomas et al., 2002).

### 6.2.2. Tectonostratigraphic evolution

The Zaisan depression developed in the Carboniferous–Permian Kalba–Naryn terrane along the Irtysh shear zone, a major tectonic boundary separating the Altai massif from the Kazakh platform (Glorie et al., 2012). It started to develop in the late Permian–Jurassic, and was active during all the Cenozoic. During this long history, sedimentation occurred in a fault-bounded grabens and the boundary faults have been active throughout all the tectonic cycles (Mekhed and Shamshikov, 1987). The sediments fill recorded a long history of deposition in a tectonically unstable setting, interrupted by a relatively short but intense period of tectonic inversion (Erofeev, 1969; Mekhed and Shamshikov, 1987). The northern boundary fault was activated in a transpressional way by the 35–40 km deep *M*<sub>s</sub> 6.9–7.0 April 14, 1990 Irtysh earthquake (Rogozhin and Leontyev, 1992). Field investigations confirmed that the basin margin is overthrust by the adjacent range along active rangeward dipping low-angle reverse faults (Fig. 10, profile A–A').

The southern side of the Zaisan basin has been progressively uplifted during late Quaternary, exposing deformed Mesozoic, Paleogene and early Neogene deposits along small transversal rivers. Examination of these sections shows that subsidence and sedimentation occurred intermittently, from Triassic to middle Jurassic and from late Cretaceous to early Pliocene. No angular unconformities between Mesozoic and Paleogene series are reported, but major tectonic deformation occurred after deposition of the early Pliocene sediments (Borisov, 1983; Erofeev, 1969). The Triassic to early Pliocene series have been folded, faulted and tilted altogether. A proluvial surface covered by thin middle-late Pleistocene conglomerate developed unconformably over the basement margin and the deformed Meso-Cenozoic sediments. This surface was uplifted and tilted progressively during the late Pleistocene–Holocene. Field observations show that a basinward dipping reverse fault affects the southern flank of the Zaisan depression, uplifting the Saikan range over the small Kenderlyk satellite basin.

These morpho-structural and stratigraphic relations suggest that the major tectonic activity in this area occurred during a restricted period of time, corresponding to the late Pliocene–early Pleistocene. After this event, a general uplift of the southern margin of the Zaisan depression relative to its northern margin, and subsequent northward tilting of the entire area occurred. No more tectonic movements were recorded along the southern boundary after the development of the middle-late Pleistocene proluvial surface.

## 6.3. Issyk-Kul basin in Central Tien Shan

### 6.3.1. Basin morphology

In the northern part of the Kyrgyz Tien Shan, Lake Issyk-Kul occupies a lens-shape tectonic depression elongated in a N80°E direction, 180 km long, 60 km wide and bordered by high mountain ranges (Fig. 8B). Its present-day lake level lies at 1607 m above sea level, and is 668 m deep with a flat bottom (De Batist et al., 2002). To the north, the Kungey Alatau range reaches 4980 m high and to the south, the Terskey range culminates at 5200 m, forming the frontal scarp of the elevated and relatively flat Kumtor Plateau at 3800–4300 high (Fig. 11).

### 6.3.2. Tectonostratigraphic evolution

The Issyk-Kul basin contains up to 6000 m of sediments (Chedia, 1986; De Batist et al., 2002). Thin deposits known as the *Kokturpack* formation were laid under relatively stable tectonic setting during the Eocene. Oligocene to early Miocene red sandstones of the *Kyrgyz* formation mark the initiation of the basin development. Since the Pliocene, sedimentation accelerated and up to 3500 m of sediments (Fortuna, 1993) accumulated in a transpressional context (Buslov et al., 2003b). The basin deepens progressively during the Pliocene, with deposition of conglomerates, sandstones and siltstone of the *Chu* formation. During the late Pliocene–early Pleistocene, concordantly with a general climate cooling, coarse molassic sediments of the *Sharpyldak* formation were

deposited during the development of low-angle thrusts along the northern and western sides of the basin (Mikolaichuk, 2000) and structural inversions along the south-western shore of the lake (Fig. 13). it was followed by late Quaternary lacustrine deposits of the *Issyk-Kul* formation.

The age of the Sharpyldak formation which constrains the timing of the tectonic intensification, is estimated between 3.5 and 1.5 Ma on the basis of a fossil horse bone and fresh water ostracods (Bullen et al., 2001; Trofimov et al., 1976).

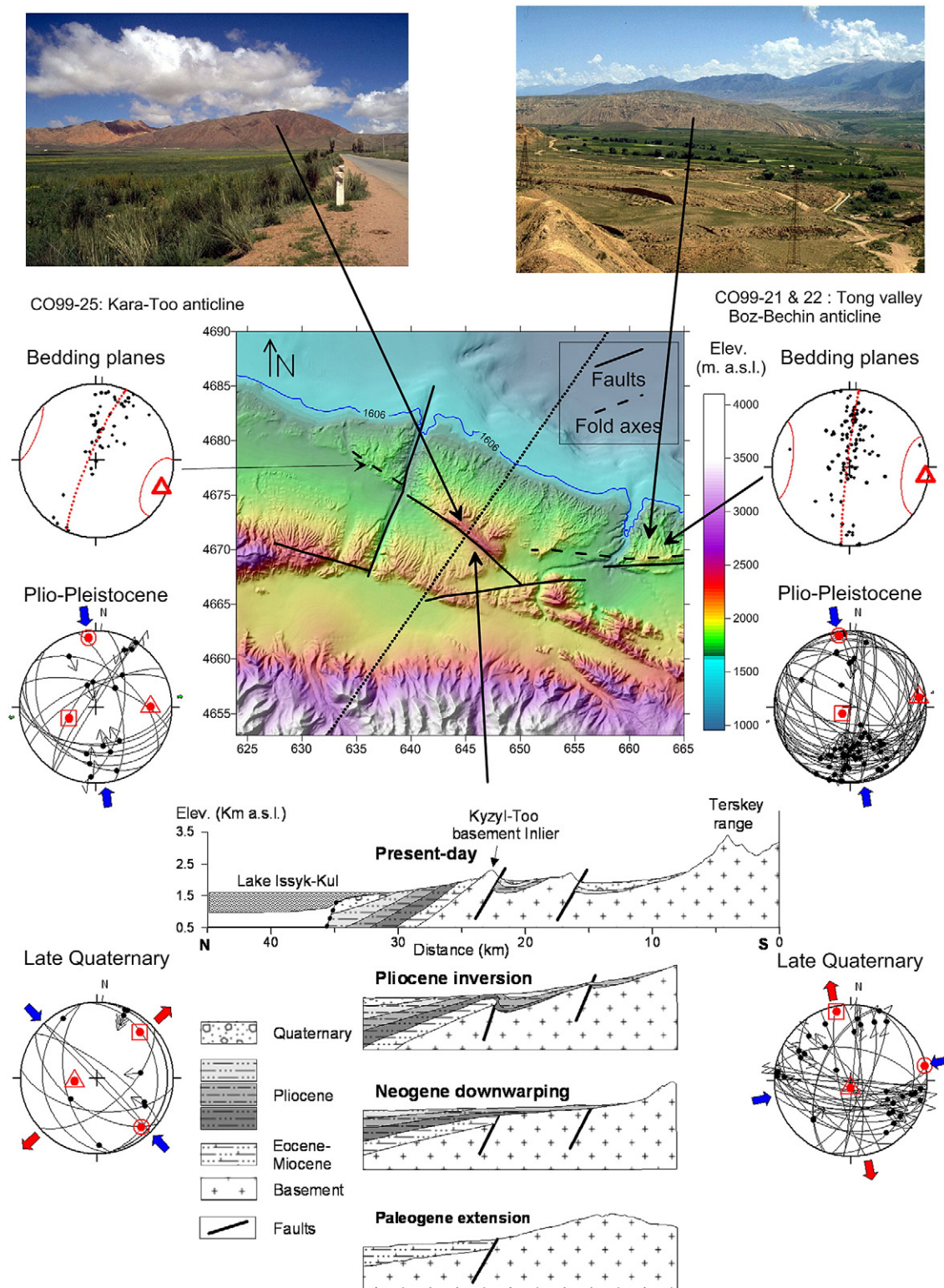


**Fig. 13.** Basement involved fault-propagation fold along the southern margin of Lake Issyk-Kul near Bokombaievskoye (site 5 in Fig. 8B). Central map: DEM constructed from digitalization of 1:50,000 topographic maps and 1:100,000 bathymetric maps by minimum curvature. Bottom panels show an interpreted section through the Kyzyl-Too basement inlier and paleostress results from the Kara-Too and Boz-Nechin anticlines, interpreted as a normal fault inverted during late Pliocene–early Pleistocene. Stereograms with fault planes as great circles, pole of bedding planes and stress results for Kara-Too (left) and Boz-Bechin (right) anticlines. The stress axes as red circle ( $\sigma_1$ ), triangle ( $\sigma_2$ ) and square ( $\sigma_3$ );  $S_{Hmax}$  as blue inwards arrows and  $S_{Hmin}$  as red outwards arrows.

The Issyk-Kul basin probably developed during deposition of the Kokturpack and Kyrgyz formations in an extensional context. This is subbed by listric faults affecting the Kokturpack formation in the northeastern side of the basin, near Toru-Aigir (Fig. 11). Additional evidence is provided by the interpretation of the basement-involved fault-propagation fold near Bokombaievskoye on the southern margin of the lake (Fig. 13). The Kyrgyz formation is limited on the northern side of the fault that formed the Kyzyl-Too basement inlier. This fault, which was initiated as a normal fault, controlled the deposition of the Kyrgyz formation and was inverted during the Neogene compression.

Around Lake Issyk-Kul, the compression direction was relatively orthogonal to the general direction of Lake Issyk-Kul and surrounding ranges during the Pliocene–early Pleistocene (Fig. 4B). The current stress stage corresponds to strike–slip reactivations along the basin marginal faults and pull-apart development within the basin itself (Abdrakhmatov et al., 2002; Buslov et al., 2003a). This two-stage evolution is well expressed in Bokombaievskoye area (Fig. 13), where the fault–propagation folds are reactivated by strike–slip movements and also in the pop-down Boom structure (Fig. 14).

### 6.3.3. Basin structure

The Issyk-Kul basin developed on the more rigid North Tien Shan block surrounded by Paleozoic accretion–collision belts. The inherited crustal heterogeneity and thermotectonic contrast (~450 Ma for the Issyk-Kul microcontinent and 300–250 Ma for the surrounding belts) likely influenced the development of the active structures, both at lithospheric and upper crustal scale.

North of the Issyk-Kul depression, the coupled Zaili and Kungey ranges mark the transition between the Kazakhstan Platform and the Issyk-Kul microcontinent (Fig. 8B). These form a positive flower structure with the Chon-Kemin–Chilik fault system in its middle. The ranges on both sides are both affected by inward dipping high-angle reverse and low-angle thrust faults. It forms a complex transpressional fault system that generated several  $M_s > 8.0$  historic earthquakes (Bogdanovitch et al., 1914; Tibaldi et al., 1997). The last one, the 1911  $M 8.2$  Kemin earthquake activated six fault segments of different strike, dip and kinematic, with surface ruptures recognized over 190 km long and numerous landslides and rock avalanches (Delvaux et al., 2001).

The Chon-Kemin fault zone is well expressed in the lower Chon-Kemin valley and in the Chu river canyon which crosscuts the entire structure in the Boom area (Fig. 14). The fault zone is associated to a pop-down prismatic basin bounded by opposite verging thrust faults, partly concealing Tertiary sediments under advancing basement margins. The pop-down basin is flanked by pop-up basement ridges on both sides, themselves thrust over the Kazakhstan platform to the North and over the Issyk-Kul depression to the South. This structure, which developed during the late Pliocene–early Pleistocene paroxysm, was later reactivated as a subvertical left-lateral strike–slip fault zone in its center.

As shown by the basement depth isolines on the geological map of the Kyrgyz republic and in Sadybakazov (1990), the Issyk-Kul depression progressively narrows and deepens eastwards, evolving from a single large downwarp into a pair of narrower parallel synclinal depressions. This folded structure affects the entire sediment thickness and is well expressed on sub-surface by an anticlinal ridge that pierce the basin floor between the Tiup and Jyrgalan rivers east of the lake. Plio-Pleistocene sediments are exposed in the core of the anticline while the rest of the plain is covered by late Quaternary deposits. In the flat bottom of the lake, bathymetric and seismic investigations evidenced the presence of an active anticlinal ridge (Vermeesch et al., 2004), similar to the one affecting the surface morphology at the eastern termination of the basin.

The Issyk-Kul basin has been interpreted as a typical ramp basin bounded on both long sides by basinward verging thrusts (Cobbold et al., 1996). However, Chedia (1986) and Sadybakazov (1990) do not describe major basinward verging thrusts on the southern rim despite

their detailed field observations. This is in line with our field observations and suggests another type of range–basin transition. Near Bokombaievskoye (Fig. 13), low lands close to the lake shore display a basinwards dipping reverse fault that caused monoclinical folding of Neogene sediments over a basement inlier which had been displaced in a brittle way. This reverse fault probably reactivates an old normal fault which controlled sedimentation during Oligocene–Miocene times. Other minor basinward dipping reverse faults can be seen at several locations along the southern margin of the basin, together with bedding parallel slip movements. In addition, the entire southern margin of the basin appears tilted basinward at the foot of the Terskey range. This is best expressed at the unconformity of the Paleogene sediments over the former Cretaceous peneplain surface (Fig. 10). This surface, which should have been originally subhorizontal, is now markedly tilted basinwards, with an increasing inclination towards the central part of the basin margin, reaching 60°N along the Tosor valley, East of Kadji-Say (Fig. 12, picture B). Inclination of the overlying sediments decreases progressively away from the basin margin and with decreasing stratigraphic age. In this area, deformation and tilting do not appear to be driven by rangeward dipping reverse faults.

Geodetic data compiled by Buslov et al. (2007) show that the southern margin of the depression is uplifting at a rate reaching 2.4 mm/yr, in accordance with the progressive lake level regression which causes the emergence of the Neogene sediments along the southern lake shore. In contrast, along the northern shore, a geodetic subsidence of 2 to 3.7 mm/yr has been measured, and Neogene sediments are buried under the Quaternary.

### 6.3.4. Topographic undulations south of the depression

South of the Issyk-Kul depression, the Terskey range forms a rugged transition from the 1600 m high lake shore to the 3800–4300 m high Kumtor plateau. The latter corresponds to remnants of the former Cretaceous peneplain, now appearing as an undulating surface with well preserved lows covered by thin ice sheets and grading southwards to the 5125 m high Ak-Siyrak–Kalyu range. (Fig. 12, pictures C, D). Close to the plateau margin, the former peneplain surface rises progressively into an asymmetric range with a gently south dipping southern slope (the preserved peneplain) and steep cliffs on the northern slope (Fig. 12, picture A). The gentle dipping southern slope at the edge of the Kumtor plateau could represent the southern flank of a broad asymmetric crustal anticline, while the steep north-dipping remains of the peneplain surface under the tilted Paleocene sediments along the margin of the depression could form the steep northern flank of that anticline. In between, the rugged Terskey Mountains correspond in this view to an eroded anticlinal bulge.

A complex system of minor faults in the crustal antilinal might accommodate the flexural deformation, but no clear evidence exist for a single major crustal scale reverse fault that would cause thrusting of the basement range onto the basin margin. If that was the case, the sediments from the basin margin should be downflexed towards the range, but instead they appear to rise progressively.

### 6.3.5. Megafold pairs

The Kumtor plateau, Terskey range upwarp and Issyk-Kul downwarp define together a large “megafold” pair, forming a succession of a broad asymmetrical anticline and a large syncline (Figs. 8b, 9b). Similarly, the Pobedy massif at the border between Kyrgyzstan, Kazakhstan and China is a broad uplift culminating at 7440 m, formed by the merging of several mountain ranges. It develops where the Tien Shan ranges gets narrower, probably by over-amplification and merging of upper crustal folds into a broad anticline.

### 6.3.6. Brittle versus buckling deformation

The distribution of seismic epicenters shows a low seismic activity underneath Lake Issyk-Kul but highly active seismic belts along its southern shore and along the Chon-Kemin–Chilik fault zone in the

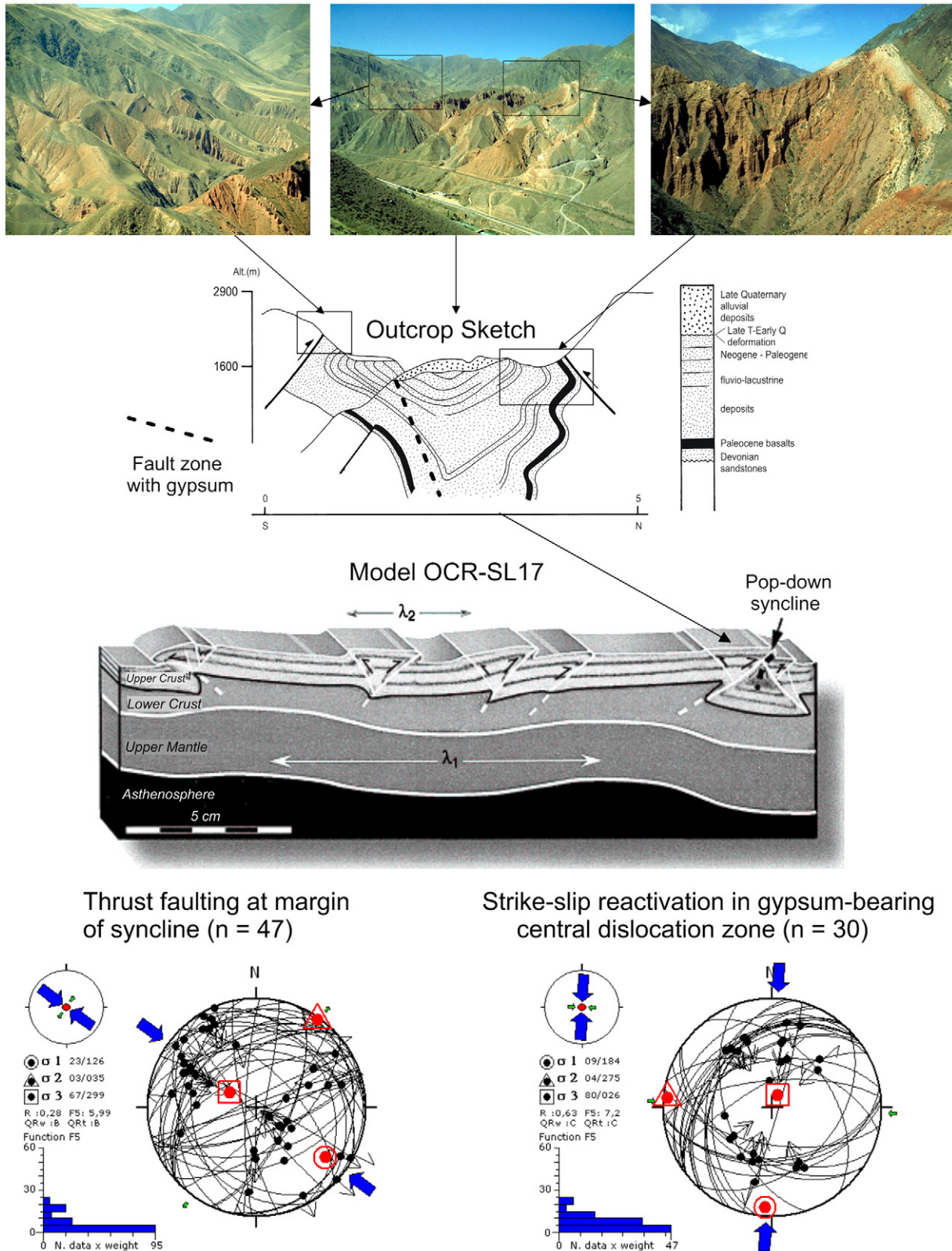


**Fig. 14.** Pop-down syncline near Boom (site 6 in Fig. 8B). Top part: field views and outcrop sketch, central part: comparison with analogue model OCR-SL17 of Sokoutis et al. (2005). Bottom: paleostress tensors from fault-slip data collected at the thrust margins (a) and from a younger central dislocation zone (b). Symbols as in Fig. 13, histograms for the misfit function.

Kungey range (e.g. Tychkov et al., 2008). The GPS-derived velocity field show in contrast that the N-S shortening is localized below Lake Issyk-Kul with an accelerated convergence of 4–6 mm/yr, continuing further to the WSW until the Talas-Fergana fault zone

(Abdrakmatov et al., 1996; Meade and Hager, 2001; Zubovich et al., 2001). Together, Abdrakmatov et al. (2001) and Meade and Hager (2001) consider that this relative movement is absorbed by major faults bounding rigid blocks, but Zubovich et al. (2001) show

that it is focused in the lake. This suggests that the Issyk-Kul depression is deforming internally by downwards buckling and that its 4–6 mm/yr of N–S shortening cannot be solely attributed to brittle movements on the basin boundary faults. This is supported by the presence of active anticline folding in the lake floor and in the eastern side of the depression as revised above.

Our interpretation contrasts with the suggestion of Thompson et al. (2002) that upper crustal deformation and seismicity in the Kyrgyz Tien Shan concentrates along a small number of major fault zones close to the basin margins, as illustrated by the Kyrgyz range–Chu basin transition near Bishkek (Bullen et al., 2003) and further east but before the Issyk-Kul depression (Abdrakhmatov et al., 2001). For this region, deformation could be dominated by slip along large crustal-scale reverse faults (Abdrakhmatov et al., 2001; Bullen et al., 2001, 2003; Ghose et al., 1997). Instead, for the Issyk-Kul region, we favor a deformation model by lithospheric-scale flexural folding accommodated by upper crustal faulting. If both interpretations are correct, this would evidence a marked lateral change, with dominant crustal faulting in the Kyrgyz range and lithospheric folding in the Issyk-Kul region. The decoupling between these two sectors corresponds to a complex transversal tectonic zone located at the western termination of Issyk-Kul basin.

## 7. Basin evolution in a folding lithosphere

Characteristic features of basins developing on a folding lithosphere (FLB) have been synthesized by Cloetingh and Burov (2011) using examples from Central Asia (Fergana and Tadjik basins) and Europe. Basin shape, architecture and symmetry, vertical motions, thermal regime and faulting activity differentiate the FLB from other types (Cloetingh and Ziegler, 2007). The Issyk-Kul, Zaisan, Kurai and Chuya basins that formed in a combination of lithospheric-scale folding and upper crustal faulting under far-field compressional stresses are examined in this perspective.

Using the remnants of the late Mesozoic–early Cenozoic planation surface, we assume that the prominent topographic ranges and basins or depressions represent lithospheric anticlines degraded by erosion and synclines partly filled by late Cenozoic sediments. Together with the late Cenozoic fault systems, they form the surface expression of lithospheric deformation. Comparison of these neotectonic elements (Fig. 4A–B) with the basement terrane architecture (Fig. 3A–B) highlights the influence of the major basement structure on the development of folding and faulting instabilities.

### 7.1. Time frame, shortening and strain rate

The shortening rate and the total amount of shortening of the lithosphere are two important parameters in the development of folds in a compressed lithosphere as they control the development of their characteristic wavelength and amplitude (Cloetingh et al., 1999; Martinod and Davy, 1994). We have shown that in Central Asia, folding of the lithosphere and the associated upper crustal faulting developed mainly during the late Pliocene–early Quaternary period of maximum tectonic compression. With the knowledge of the deformation history, the present-day GPS N–S shortening rates and assuming the total shortening across the belts, the duration and shortening rate for this period can be estimated.

In the Altai belt, the onset of late Cenozoic relief rejuvenation is estimated at 5 Ma (De Grave et al., 2007a, 2007b; Vassallo et al., 2007). In Tien Shan, the onset of crustal shortening (Abdrakhmatov et al., 1996) and rapid exhumation (Bullen et al., 2001) are both estimated at ~10 Ma. In these two belts, the beginning of major compression stage is constrained stratigraphically at ~3.5 Ma and the transition to the neotectonic relaxation stage, at ~1 Ma. The time-scale associated with the major shortening stage that caused folding of the lithosphere and most of the faulting is therefore very short (2.5 Ma). This is typical for

FLB (Cloetingh and Burov, 2011). The period of initial shortening is therefore 1.5 Ma long for the Altai belt and 6.5 Ma for the Tien Shan (Table 3).

The GPS velocity field shows a general N–S direction of shortening, in accordance to the present  $S_{Hmax}$  stress trajectories deduced from earthquake focal mechanisms and from late Quaternary brittle structures. The present-day shortening rate was estimated at 10–12 mm/yr across the Altai (Goldin et al., 2005) and 17–18 mm/yr across the Tien Shan (Calais et al., 2003, 2006). Inferring that these values characterize the Neotectonic relaxation period, the shortening rate must have been higher during the period of major tectonic shortening. The Altai and Tien Shan belts have a present width respectively of 800 and 400 km and we assume corresponding amounts of late Cenozoic shortening to respectively 100 and 200 km. Using average shortening rates of 11 mm/yr for the Altai and 17.5 mm/yr for the Tien Shan, the corresponding strain rates are therefore respectively  $1.2 \times 10^{-8} \text{ yr}^{-1}$  and  $2.9 \text{ in} \times 10^{-8} \text{ yr}^{-1}$  (Table 3).

We then determined the possible shortening rates for the major compression period, and their corresponding amount of shortening. The shortening rates for the major compression stage should be faster than the shortening rates during both the neotectonic relaxation stage and the initial compression stage, and the resultant shortening for the initial stage cannot be negative. The possible shortening rates for the major compression period are therefore between 23 and 35.5 mm/yr for the Altai (2.1 to 3.2 times the shortening rate for the neotectonic stage) and between 17.5 and 71.5 mm/yr for the Tien Shan (1 to 4.1 times). For both belts, we propose 2 scenarios for this period (Table 3); with a faster shortening (30 and 35 mm/yr) and slower shortening (25 and 30 mm/yr). The corresponding amount of shortening and shortening rates for the initial compression stage are obtained using the total amount of shortening across the range and the estimated duration for the initial stage.

For Altai–Sayan, the faster scenario (30 mm/yr shortening rate,  $3.3 \times 10^{-8} \text{ yr}^{-1}$  deformation rate) is preferred as it gives a slow deformation rate during the initial period ( $1.0 \times 10^{-8} \text{ yr}^{-1}$ ), which is compatible with the small amount of deformation that apparently occurred before the onset of major compression. For the Tien Shan, the slower scenario is preferred (30 mm/yr,  $5 \times 10^{-8} \text{ yr}^{-1}$ ), in order to ensure a sufficiently high deformation rate during the initial compression period ( $2.8 \times 10^{-8} \text{ yr}^{-1}$ ) to allow significant denudation and sedimentation that was evidenced for the late Miocene–early Pliocene.

### 7.2. Stress field and lithospheric folding trend

Nikishin et al. (1993) and Burov et al. (1993) were the first to present a regional study of the continental lithospheric folding in Central Asia on the basis of geological and topographic observations and Bouguer gravity data. They evidenced two characteristic dominant wavelengths of ~50 and 300–360 km, interpreted as reflecting independent quasi-viscous folding, respectively of strong upper crust and of the whole lithosphere. On the basis of the limited number of focal mechanisms available at the time, a transpressional setting with a general NE  $S_{Hmax}$  was assumed. A partition of deformation into a combination of shortening and strike-slip is not envisaged for the studied regions as this is not supported by earthquake focal mechanisms, fault-slip data nor GPS deformation field. They further showed that the axes of the large scale uplift and subsidence zones which were assumed to reflect lithospheric mantle folding are trending NW–SE, at a high angle to the E–W crustal-scale folds defined by the 30–50 km spaced linear basins and ranges.

This oblique relation between the upper crustal and lithospheric mantle folding is not confirmed here. Instead, the axial direction of the lithospheric folds tends to be sub-orthogonal to the  $S_{Hmax}$  direction of the late Pliocene–early Pleistocene. This is clearly evidenced for the Tien Shan, where the lithospheric folds formed at a high angle to the N130°E oriented  $S_{Hmax}$ . In Altai–Sayan, where the

**Table 3**  
Distribution of late Cenozoic lithospheric shortening and strain rate for the 3 development stage of folded lithospheric basins in Tien Shan and Altai–Sayan. From (a) Abdrakhmatov et al. (1996); (b) Bullen et al. (2001), (c) Delvaux et al., 1995c), (d) own field structural and paleostress data, (e) Calais et al. (2003, 2006) and Goldin et al. (2005). Details in text. Gray background: preferred scenario for the major compression stage and corresponding scenario for the initiation stage.

Time constraints	Tectonic periods				Altai–Sayan belt				Tien Shan belt				
	Timing (TS/AS)		Duration (TS/AS)		Tectonic periods	Short. rate	Lith. short.	Strain rate	Cum. short.	Short. rate	Lith. short.	Strain rate	Cum. short.
	Ma	Ma	Ma	Ma		mm/yr	km	10–8 yr <sup>-1</sup>	%	mm/yr	km	10–8 yr <sup>-1</sup>	%
Onset crustal shortening (a) & rapid exhumation (b)	5	10	1.5	6.5	Initial compression	17.7	26.58	2.0	4	4.0	107.47	2.8	18
Older age for Sharpyldack fm in Issyk-Kul (b) and Becken fm in Chuya (c) basins	3.5		2.5		Major compression	9.4	14.06	1.0	1	3.6	95	2.4	14
End of strong tectonic compression, begin of Neotectonic period (d)	1		1		compression	30.0	74.94	3.3		35.0	87.5	5.8	
Present-day GPS N–S shortening rates (e)	0				Neo-tectonic relaxation	11.0	11	1.2	11.1	17.5	17.5	2.9	33.3
Estimated total shortening (km)						100				200			
Present width (km)						800				400			
Initial width (km)						900				600			
Normalized shortening (total shortening/initial width, %)						11.11				33.33			

basement structure is more complex and heterogeneous, the folding axes appear less well controlled by the  $S_{Hmax}$  direction as they tend to align with the major faults and old shear zones.

Lithospheric folding is studied here using topographic-structural sections constructed in parallelism with the  $S_{Hmax}$  directions for the period of most intense shortening. Despite the different orientation of the profiles, the wavelength spectra obtained are relatively similar to those of Nikishin et al. (1993) and Burov et al. (1993) and reflect also a combination of mantle and upper crustal folding.

### 7.3. Folding wavelength and crustal structure

Numerical modelling (Cloetingh and Burov, 2011) showed that lithospheric folding is best developed for intermediate aged lithosphere (300 Ma), leading to long mantle wavelengths (360 km) with high surface amplitude. At the same time, the upper crustal wavelength ranges from 50 to 150 km.

The Fourier Transform analyses of the topographic profiles (Fig. 6, Table 2a) show that for Altai–Sayan, the long wavelengths are in the range of 200–300 km and in Tien Shan, 200–350 km. The short wavelengths are 40–60 km for Altai–Sayan and 70–80 km for Tien Shan. Intermediate wavelengths of 110–170 km are observed in the two regions, possibly representing interference patterns, the influence of pre-existing crustal scale discontinuities or the presence of competent intermediate or lower crustal layers.

The lateral variations of wavelength spectra observed in Altai–Sayan could reflect crustal heterogeneity. Long wavelength folds are well expressed in western Altai (Kalba–Narym and Rudny Altai Carboniferous–Permian terranes), while in the east (West-Sayan and Gorny–Altai Vendian–Cambrian terranes with granitic intrusions), long wavelength folding is replaced by short wavelength folding. This suggests a shift from upper mantle dominated buckling in the west to upper crustal dominated deformation in the east. North of the Altai range, lithospheric folding ceases when reaching the Western Siberian plate.

In Tien Shan, the wavelength spectra also show lateral variations, with long wavelengths of 150–200 km across Issyk-Kul basin and 250–350 km for the Pobedy massif and Tekes basin. The presence of intermediate wavelengths and the relatively poor expression of short wavelengths in the Tien Shan might be due to crustal changes along the topographic profiles. Along the same profiles, different wavelengths develop according to changes in the crustal structure. For the profile C–C' (Fig. 12) across Issyk-Kul basin, large amplitude (up to 8 km) relatively long wavelength (~150 km) folding of the pre-Cenozoic planation surface develop in the early Paleozoic

Issyk-Kul microcontinent (450–400 Ma) while smaller amplitude (1–2 km) shorter wavelength (40–50 km) develop in the late Paleozoic Central Tien Shan highlands (300–250 Ma).

In the southern margin of the Kazakhstan platform, folding amplitude progressively decreases northwards while wavelength increases together with thermotectonic age (from 300 to 450–480 Ma). Tectonic loading at the margin of the Tien Shan might be responsible for a very long wavelength and small amplitude undulation seen in the platform further north. Similarly, no true lithospheric folding is observed in the Tarim platform (750 Ma), but its margins were nevertheless deformed by tectonic loading from the Kunlun range on the south and Tien Shan on the north (Yang and Liu, 2002).

### 7.4. Folding amplitude and shortening rate

Amplitude of lithospheric folds in the Altai–Sayan and Tien Shan belts fluctuates across the ranges, with maxima not necessarily at the center of the belts. Minimum amplitudes can be estimated using the elevation difference between the base of the basin fill and the top of the adjacent ranges. In Altai, large amplitudes are observed for the Zaisan basin/Tarbagatai range (3.8–4.2 km) and for the Kurai ridge/Chuya basin/South-Chuya range (3–4 km). For the Tien Shan, the largest folding amplitude is attained for the Issyk-Kul basin/Kungey range megafold (7.5–8 km) and the Pobedy range between the Tekes basin and the Tarim platform (>7 km). This two-fold difference in maximum amplitude cannot be related to the two-fold difference in the estimated shortening rate across the ranges during the period of major compression (2.8–3.3 versus  $5.0\text{--}5.8 \times 10^8 \text{ yr}^{-1}$ ), because wavelength and amplitude for lithospheric folding are more controlled by the thermo-mechanical age of the lithosphere than by the rate of shortening (Cloetingh and Burov, 2011). At large amounts of shortening, deformation may become aperiodic so that the wavelength and amplitude of folding vary across the deformed belt (Hunt et al., 1996). Gravity-dependent numerical modeling results (Cloetingh and Burov, 2011) also show that folding becomes aperiodic at later stages (after 10 Ma in their model), leading to mega-folding and the formation of high-amplitude crustal down- and up-warps with over-amplified vertical movements that may reach 10–20 km. So the higher folding amplitude recorded in Tien Shan than in Altai might reflect longer deformation (10 Ma vs 5 Ma) and/or larger percentage of shortening along the sections (33% vs 11%; Table 3).

In the models of Burg and Podladchikov (1999) and Cloetingh et al. (1999), aperiodic megafold develop at large amounts of shortening (20–50%) due to non-linear rheology, conjunction of several short wavelength folds and lower crustal flow. Megafolds such as the

Issyk-Kul basin and Pobedy massif in the Tien Shan are not observed in Altai–Sayan, where the cumulative shortening at the end of the major compression stage reaches only 10% while it reaches 30% in Tien Shan (Table 3).

### 7.5. Faulting and folding

During lithospheric folding, faulting did not impede the development of buckling instabilities but participates to it (Cloetingh et al., 1999; Gerbault et al., 1999). Sedimentary basins in this context evolve partly by flexure and folding and partly by fault-controlled deformation. In the Altai–Sayan and Tien Shan case studies, fault-controlled deformation alone is largely insufficient to explain the observed tectonic morphology. Upper crustal deformation appears dominated by surface tilting, uplift and subsidence in response to lithospheric buckling.

In Altai–Sayan, the short wavelength topographic buckles are partly controlled by thrust faulting or by oblique–reverse faulting and block tilting. The 2000 m step between the South–Altai range and the Bukhtarma valley is controlled by a strong reverse faulting amplification of a crustal fold. Further east, the South Altai range is connected to the Tolbo–Nur strike–slip fault in Mongolia and has been interpreted as a thrust termination of a large strike–slip system (Bayasgalan et al., 1999). The Kurai fault system that forms the northern boundary of the Kurai–Chuya basin system is part of a positive flower structure (Bondarenko, 1976; Delvaux et al., 1995c). The other ranges in Gorny Altai and Rudny Altai seem mainly unrelated to fault systems.

In high-altitude Central Tien Shan, the topographic undulations are apparently unrelated to major fault lines, while at the margin of the Issyk–Kul basin, faulting accompanies lithospheric folding. The Issyk–Kul basin has been described as a ramp basin by Cobbold et al. (1993), but a re-inspection of the evidence provided by Sadybakazov (1990) combined with new field observations show that faulting contributes only to a small extent to the differential vertical movements between the basins and the ranges. Basinward tilting of the former planation surface on the sides of the basin is the dominant relief producing mechanism (Fig. 12). It can be accompanied by complex minor faulting in the basement and by rangeward-directed minor faults in the basin fill. This structural style is also expressed further east (Pobedy massif, Tekes basin, Ili depression, Borohoro range in Kazakhstan), but at the transition between the Tien Shan and adjacent platforms, low-angle thrusting dominates, creating foreland basins.

In both case studies, folding and faulting coincide when they are associated to positive flower systems along transpressional fault systems (Hovd–Shapshal and Kurai fault systems in Altai–Sayan and Chon–Kemin–Chilik fault system in Tien Shan). They coexist also in the over steepened flanks of strongly amplified lithospheric folds (e.g. eastern extremity of Issyk–Kul basin), where faulting becomes a more efficient way for further shortening than additional tilting. Otherwise, faulting and folding tend to occur in a mutual exclusion. Brittle thrusting also develops in the inflexion points of synclines, leading to pop-down structures as in Boom in the Tien Shan.

### 7.6. Modes of lithospheric folding

As shown by e.g. Cloetingh et al. (1999), different modes of lithospheric folding in a stratified lithosphere might occur in function of the lithospheric structure and rheology: upper crustal folding (monoharmonic), lithospheric mantle folding (biharmonic, decoupled) and whole lithosphere folding (monoharmonic, coupled). These 3 modes of folding control the wavelength which appears as progressively longer from upper crustal to whole lithospheric folding. The combination of long (200–350 km) and short (40–70 km) wavelengths observed in the Tien Shan and Altai–Sayan belts suggest that both the upper crust and upper mantle are folded in a biharmonic decoupled mode.

For the Tien Shan, Bragin et al. (2001) and Tychkov et al. (2008) showed that the Moho is 5–7 km deeper beneath the Issyk–Kul depression than under the neighboring areas. Similarly, seismic tomography (Bushenkova et al., 2002) and gravity data (Artemeviev et al., 1993) suggest the presence of a cold lithosphere beneath the lake, while a hotter mantle could rise under most of Central Tien Shan. Heat flow modeling also supports a lithospheric folding model for the Issyk–Kul basin (Vermeesch et al., 2004). Cloetingh and Burov (2011) interpret the Issyk–Kul basin, however, in terms of typical crustal-scale folding. We have shown above that it appears as a megafold formed by the merging of several smaller amplitude undulations. As the Moho seems to be also affected, the Issyk–Kul basin could develop by the conjunction of several crustal folds that merge together, superimposed over a longer wavelength upper mantle deflection.

### 7.7. Thermal regime

Heat flow studies at regional scale in Altai–Sayan (Duchkov et al., 2010; Sokolova and Duchkov, 2008) and Tien Shan (Duchkov et al., 2001; Vermeesch et al., 2004) as at basin scale in Lake Issyk–Kul (Vermeesch et al., 2004) show that all these regions have relatively low heat flow (respectively 45–50 mW/m<sup>2</sup>, 50 ± 15 mW/m<sup>2</sup> and 54 mW/m<sup>2</sup>). This suggests a “cold Cenozoic orogeny” with no initial heating associated to tectonic deformation and basin development, as proposed for FLB (Cloetingh and Burov, 2011).

### 7.8. Comparison with lithospheric-scale analogue models

Shortening of analogue lithospheric-scale models allow to reproduce the structures that appear during continental collision and to investigate the role of lithospheric rheology and heterogeneities. By shortening a 3-layers lithosphere with a strong upper mantle and two contrasting blocks bounded by a lithospheric suture, Sokoutis et al. (2005) produced in their OCR–SL15 model a first-order deep syncline which is folding the equivalent geological Moho and is flanked by a broad anticline in the form of a megafold pair (Fig. 12). In this model, the lithospheric suture focused the basin location and the strong upper mantle favored the development of a megafold pair, with a syncline in the thicker lithosphere and a broad anticline in the thinner lithosphere. Although no lithospheric scale suture is known beneath Lake Issyk–Kul, this geometry compares well with that of the Issyk–Kul depression in the older North Tien Shan terrane, flanked by the Terskey range–Kumtor asymmetric broad anticline in the younger Central Tien Shan terrane.

In an advanced stage of the OCR–SL15 modelling experiment of Sokoutis et al. (2005), a basin became squeezed between the two flanks of the syncline that become progressively steeper. In order to accommodate the space reduction inside the basin, complex wedging of the sediments occurs with internal folding and reverse faulting that tend to expulse the sediments towards the basin margin. This kind of internal basin structure is typically what is found along the southern margin of Lake Issyk–Kul, in the Kadji–Sai area (Fig. 15). A small-scale extrusion anticline is well exposed along a transpressional fault that affects the Cenozoic and Mesozoic sediment near the margin of the basin, in which Jurassic shales were injected along the fault zone, piercing the overlying Neogene sediments.

When the lithosphere is uniformly thick, a frequent surface expression of shortening occurs in the form of fault-controlled pop-up and pop-down structures and inverted basins (Cobbold et al., 1993). Such structures are well expressed along the left bank of the Chu river canyon at the Boom site (Fig. 14) where a pop-down prismatic basin is delimited by two conjugate downward convergent thrusts. In the OCR–SL17 model of Sokoutis et al. (2005) which represents a cold lithosphere with a relatively strong mantle, the lower mantle buckles with a first-order wavelength while the prismatic pop-ups

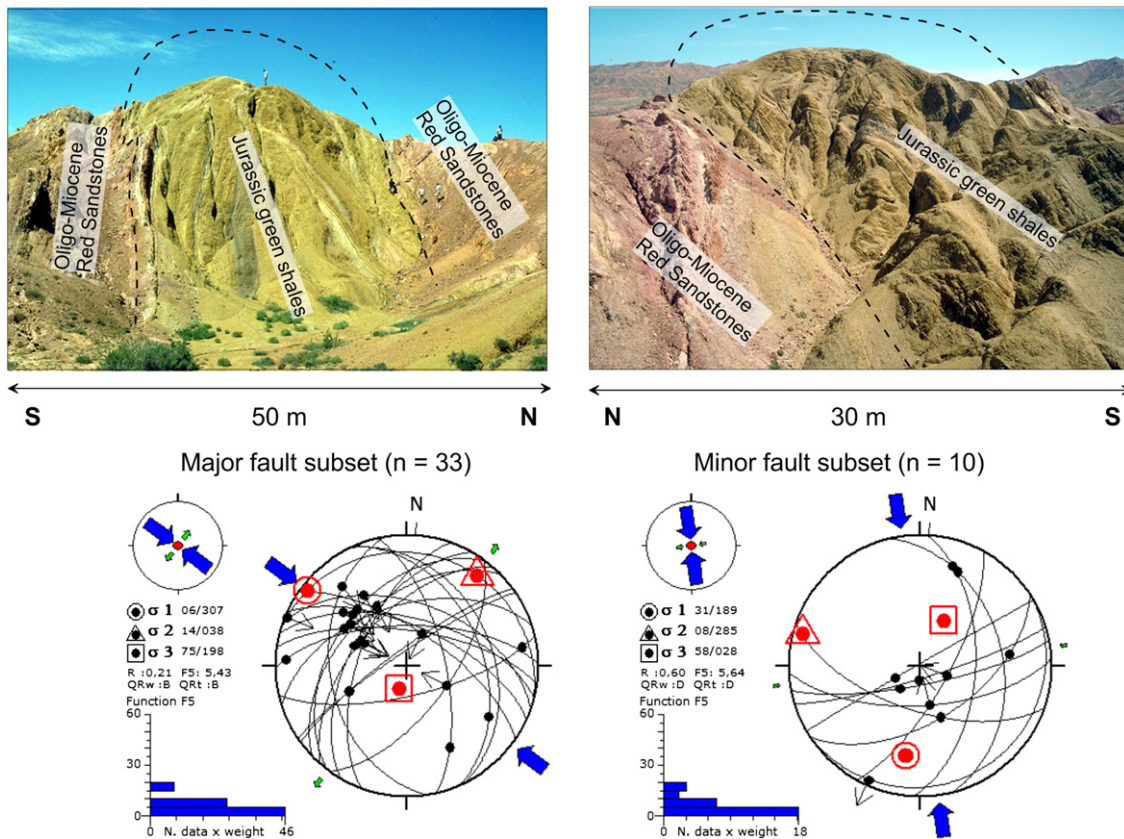


**Fig. 15.** Upward extrusion of soft green Jurassic shales into Oligocene–Miocene red sandstones of the Kyzylgyr formation along a transpressional fault zone at Kadji-Sai (site 7 in Fig. 8B). View from both sides of the same hill. Paleostress tensors from fault–slip data collected at the contact between the shales and the sandstones. Symbols as in Fig. 13, histograms for the misfit function.

and downs form in the brittle upper crust, defining a second-order wavelength.

### 7.9. Basin symmetry

Basins in a folding lithosphere generally form as symmetric isostatically “overcompensated” down-warps flanked by up-warps of similar amplitude and wavelength, in contrast with the strongly asymmetrical shape of foreland basins (Burov and Molnar, 1998). In the basins studied, this seems strictly the case only for the Kurai basin, which developed as a full-ramp basin. The Issyk-Kul basin which developed as a megafold with a high-amplitude crustal downwarp looks also at first sight symmetrical. However, our morphological and geodetic observations show that its northern margin is subsiding and accumulating late Quaternary sediments, while the southern shore is uprising and the Miocene to early Quaternary sediments are eroded.

The Chuya and Zaisan basins are now strongly asymmetrical. They developed initially as symmetrical extensional basins, but evolved asymmetrically during the compressional reactivation due to strain localization at the inflection points of the early buckles on their northern side, leading to reverse faulting associated to transcurrent movements. This could have been controlled by the combined presence of a pre-existing basement discontinuity and a transpressional rather than an orthogonal shortening context. In all the studied basins, the syn-folding depocenter remained located over the initial (pre-folding) depocenter, and this contributes to the vertical amplification of the sedimentary infill. For these basins, only a single and relatively short folding wavelength is observed, suggesting a dominant control by crustal folding (Cloetingh et al., 1999).

### 7.10. Basin closure

During the proposed 3 stage evolution model for FLB, the basins tend to evolve as closed systems during the second stage (maximum shortening) and are captured and drained out during the last stage (Cloetingh and Burov, 2011). The Kurai and Chuya basins accumulated late Pliocene–Quaternary sediments in limited thickness and are presently drained by the Chu River. They temporarily evolved as closed basin during glacial times, due to the ice-damming of the Chuya River. The breakage of the dam during the last deglaciation caused a catastrophic runoff that flushed a large volume of sediments out of the system (Rudoy, 2002). The Zaisan depression is drained by the Irtysh River and partly occupied by the shallow Lake Zaisan but the Issyk-Kul basin is still closed. It contains the world’s fifth deepest fresh water lake on earth (668 m deep max.) and has presently no outlet. The Chu River which was intermittently flowing into the western tip of the lake, is now avoiding it (De Batist et al., 2002), transferring directly the sediments from the western termination of the basin to the Chu foreland basin. The lake basin has a flat bottom and the sediment supply is too weak to fill it. Now the water level is close to the overflow sill, but it strongly fluctuated as shown by a prominent paleo-shore line 110 m under the present water level and several others above. The Tekes basin in Kazakhstan which has a similar shape as the Issyk-Kul basin is already overfilled.

### 7.11. Basin sediment fill

Basins developing in a folding lithosphere are characterized by a rapid deposition of large sediment thicknesses (Cloetingh and Burov, 2011). In the Chuya basin, late Pliocene–early Pleistocene molassic sediments (Terek and Bashkaus formations) accumulated rapidly along the

northern margin in association with the Kurai range uplift. In the Zaisan depression, 800 m of Neogene sediments have been evidenced by hydrocarbon exploration. In the Issyk-Kul basin, sedimentation accelerated markedly in Pliocene, with deposition of up to 3500 m since the beginning of the maximum shortening stage.

### 7.12. Climatic versus tectonic forcing

Relation between late Cenozoic mountain range uplift and global climate change has long been noticed worldwide (e.g. [Champagnac et al., 2012](#); [Molnar and England, 1990](#)). This could lead to a positive feedback action, promoting range uplift by fast erosion unloading and basin subsidence by fast sediment accumulation, and also preventing subsurface collapse through a mechanism as proposed by [Avouac and Burov \(1996\)](#).

In Central Asia, there is a remarkable coincidence between the acceleration of tectonic shortening and amplification of basin downwarp/range upwarp with the global climate cooling in the Plio-Pleistocene transition and the onset of Quaternary glaciations. In the Issyk-Kul basin, the Sarpyldack formation contains a large amount of coarse clastics and locally huge boulders, suggesting a glacial environment of deposition. At the foot of the Karakorum Mountains along the western margin of the Tarim basin, similar coarse clastic deposit but in much greater thickness are also known during the Pliocene, reflecting the onset of the Tibet plateau uplift ([Zheng et al., 2000](#)). A similar observation was made along the Altyn Tagh fault at the northern margin of the Tibet Plateau, where [H. Chang et al. \(2012\)](#) evidenced by magnetostratigraphy a marked change in depositional facies at ~3.2 Ma, accompanied by a remarkable increase in sedimentation rate which they attribute to a change in tectonic activity. In Central Himalaya, [Wang et al. \(2012\)](#) relate also major change in drainage systems and depositional settings at ~7.2, ~5.5 and ~3.2 Ma, to large-scale tectonic changes.

## 8. Conclusions

Central Asia is a classical example for intracontinental lithospheric folding in reaction to compressional tectonic stress of far-field origin. In particular, the Altai–Sayan belt in South-Siberia and the Kyrgyz Tien Shan display a special mode of lithospheric deformation, involving both lithospheric folding and upper crustal faulting ([Nikishin et al., 1993](#)). The Zaisan, Kurai and Chuya basins in Altai–Sayan and the Issyk-Kul and Tekes basins in Tien Shan are typical intermountain basins developing in a folding lithosphere. Their particular characteristics and evolution stages have been examined in reference to FLB type basins determined from natural examples, theoretical and modelling results by [Sokoutis et al. \(2005\)](#) and [Cloetingh and Burov \(2011\)](#).

Both areas have a contrasting crust with a long history of accretion and collision and blocks of different thermotectonic age. They have been reactivated during the India–Eurasia convergence by a combination of far-field stresses generated at the plate boundary and buoyancy stresses generated by lateral gradients in gravitational potential energy. Thanks to the youthfulness of the tectonic deformation in this region (peak deformation in late Pliocene–early Pleistocene), the surface expression of lithospheric deformation is well documented by the topography and superficial structures. The first-order topographic wavelengths of 200–300 km in Altai–Sayan and 150–200 to 250–350 km in Tien Shan, likely reflect lithospheric mantle deformation. Secondary wavelengths between 35 and 70 km are expressed in both belts by regularly spaced E–W trending mountain ranges, alternating with late Cenozoic tectonic depressions.

Tectonic, geodetic and thermochronologic studies show that shortening and rapid exhumation started ~5 Ma ago in Altai–Sayan and ~10 Ma in Tien Shan. Structural and stratigraphic analysis of late Cenozoic deposits in intramontane basins evidence a period of intense tectonic activation and shortening between middle Pliocene

(3.5 Ma) and the end of early Pleistocene (1 Ma). During the last 1 Ma, tectonic shortening was reduced, and most folds and faults ceased to develop while new faults formed to accommodate the new (and still active) stress field. This led to a 3 stages evolution with an initial compression (1.5 Ma long in Altai–Sayan and 6.5 Ma in Tien Shan), a period of major compression (2.5 Ma long in both belts) and a neotectonic relaxation period (1 Ma long).

The intramontane basins developed during this 3 stage evolution in a similar way as the 3 stages development model for Folded Lithospheric Basins (FLB) proposed by [Cloetingh and Burov \(2011\)](#). Initiation of folding during Stage 1 (initial compression) is well developed in Tien Shan but had a short duration and limited effects in Altai–Sayan. During stage 2 (major compression), intensification of folding accompanied by faulting caused uplift and erosion of the ranges and basin subsidence with sediment accumulation in closed symmetrical basins. Stage 3 (neotectonic relaxation) corresponds to a marked relaxation of tectonic deformation together with the installation of the current deformation regime. The basins stabilized, become asymmetrical, were progressively filled, captured and drained out while the mountain ranges were increasingly eroded.

During the stage of maximum tectonic compression, deformation of the lithosphere occurred by a combination of long wavelength mantle lithospheric folding and upper crustal shorter wavelength folding with faulting. Faulting participated to the deformation but did not take over the folding process. The lithospheric folds tend to develop with their axes perpendicular to the  $S_{Hmax}$  direction of the stress field that was active at the time of their formation. The presence of pre-Cenozoic crustal faults in a heterogeneous basement localized the deformation and influenced the development of the lithospheric folds. They evidence also that crustal stress can be transmitted across a folded lithosphere.

## Acknowledgments

For this work, Damien Delvaux was supported by an ISES Invited Research Fellowship at the University of Amsterdam and by the Belgian Science Policy Action 1 program at the Royal museum for Central Africa, Belgium, with additional funds from INTAS and EC-Copernicus programmes. Support from the Siberian branch of the Russian Academy of Sciences and the Kyrgyz Academy of sciences for providing and translating documentation and organizing field work is greatly appreciated. This paper is a contribution to the IGCP project 592 Continental construction in Central Asia.

## References

- Abdrakhmatov, K.E., Aldazhanov, S.A., Hager, B.H., Hamburger, M.W., Herring, T.A., Kalabaev, K.B., Makarov, V.I., Molnar, P., Panasyuk, S.V., Prilepin, M.T., Reilinger, R.E., Sadybakasov, I.S., Souter, B.J., Trapeznikov, Yu.A., Tsurkov, V.Ye., Zubovich, A.V., 1996. Relatively recent construction of the Tien Shan inferred from GPS measurements of present-day crustal deformation rates. *Nature* 384, 450–453.
- Abdrakhmatov, K., Weldon, R., Thompson, S., Burbank, D., Rubin, C., Miller, M., Molnar, P., 2001. Onset, style and current rate of shortening in the central Tien Shan, Kyrgyz Republic. *Russian Geology and Geophysics* 42, 1609–2001.
- Abdrakhmatov, K.E., Djanuzakov, K.D., Delvaux, D., 2002. Active tectonics and seismic hazard of the Issyk-Kul basin in the Kyrgyz Tien-Shan. *NATO Science Series IV. Earth and Environmental Sciences* 13, 147–160.
- Agatova, A.R., Novikov, I.S., Vysotsky, E.M., Gibsher, A.S., 2004. Geomorphologic effects of the 27 September and 1 October 2003 earthquakes in Gorny Altai. *Geomorfologiya* 3, 3–12.
- Allen, M.B., Windley, B.F., Chi, Zang, 1992. Paleozoic collisional tectonics and magmatism of the Chinese Tien Shan, central Asia. *Tectonophysics* 220, 89–115.
- Angelier, J., 1994. Fault slip analysis and paleostress reconstruction. In: Hancock, P.L. (Ed.), *Continental Deformation*. Pergamon, Oxford, pp. 101–120.
- Arjannikova, A., Larroque, C., Ritz, J.-F., Déverchère, J., Stéphan, J.F., Arjannikov, S., San'kov, V., 2004. Geometry and kinematics of recent deformation in the Mondy–Tunka area (south-westernmost Baikal rift zone, Mongolia–Siberia). *Terra Nova* 16 (5), 265–272.
- Artemeviev, M.E., Demianov, G.V., Kaban, M.K., Kucherenko, V.A., 1993. Density contrasts in the lithospheric gravity field in North Asia. *Izvestia Akademii Nauk SSSR, Fizika Zemli* 5, 12–23.
- Avouac, J.P., Burov, E.B., 1996. Erosion as a mechanism of intracontinental mountain growth. *Journal of Geophysical Research* 101 (B8), 17747–17769.

- Babichev, A.V., Novikov, I.S., Polyansky, O.P., Korobeynikov, S.N., 2009. Modeling Cenozoic crustal deformation in Gorny Altai. *Russian Geology and Geophysics* 50, 104–114.
- Bagdassarov, N., Batalaev, V., Egorova, V., 2011. State of lithosphere beneath Tien Shan from petrology and electrical conductivity of xenoliths. *Journal of Geophysical Research* 116, B01202 (22 pp.).
- Bayasgalan, A., Jackson, J., Ritz, J.-F., Carretier, S., 1999. Field examples of strike–slip fault termination in Mongolia and their tectonic significance. *Tectonics* 18 (3), 394–411.
- Berzin, N.A., Coleman, R.G., Dobretsov, N.L., Zonenshain, L.P., Xuchang, Xiao, Chang, E.Z., 1994. Geodynamic map of the western part of the Paleo-Asian Ocean. *Russian Geology and Geophysics* 35 (7–8), 2–22.
- Biot, M.A., 1961. Theory of folding of stratified viscoelastic media and its implications in tectonics and orogenesis. *Geological Society of America Bulletin* 72, 1595–1620.
- Bogdanovitch, K.I., Kark, I.M., Korolkov, B.Ya, Musketov, D.I., 1914. Earthquake in the Northern Districts of the Tien Shan, 22 December 1910 (4 January 1911). Commission of the Geology Committee, Leningrad (256 pp. (in Russian)).
- Bondarenko, P.M., 1976. Modelling of overthrust dislocations in the folded areas. (On the example of Aktash structures in Gorny-Altai) *Nauka, Novosibirsk* (116 pp. (in Russian)).
- Borisov, B.A., 1983. Paleogene Biostratigraphy of the Zaysan Depression. Phanerozoic stratigraphy of the USSR. VSEGEI Publ., Leningrad, p. 322.
- Bragin, V.D., Batalaev, V.Yu., Zubovich, A.V., Lobachenko, A.N., Rybin, A.K., Trapeznikov, Yu.A., Schelochkov, G.G., 2001. Signature of neotectonics movements in the geoelectric structure of the crust and seismicity distribution in Central Tien Shan. *Russian Geology and Geophysics* 42, 1527–1537.
- Brezhnev, V.D., 1995. Age and structure of the Tarim basement. *Doklady Akademii Nauk, Earth Sciences* 335A (3), 87–92.
- Bullen, M.E., Burbank, D.W., Garver, J.I., Abdрахmatov, K.Ye., 2001. Late Cenozoic tectonic evolution of the Northwestern Tien Shan: new age estimates for the initiation of mountain building. *GSA Bulletin* 113 (12), 1544–1559.
- Bullen, M.E., Burbank, D.W., Garver, J.I., 2003. Building the Northern Tien Shan: integrated thermal, structural and topographic constraints. *Journal of Geology* 111, 149–165.
- Burg, J.P., Podladchikov, Y., 1999. Lithospheric scale folding: numerical modeling and application to the Himalayan syntaxes. *International Journal of Earth Sciences* 88, 190–200.
- Burg, J.P., Davy, P., Martinod, J., 1994. Shortening of analogue models of the continental lithosphere: new hypothesis for the formation of the Tibetan plateau. *Tectonics* 13, 475–483.
- Burov, E.B., Cloetingh, S., 1997. Erosion and rift dynamics: new thermomechanical aspects of post-rift evolution of extensional basins. *Earth and Planetary Science Letters* 150, 7–26.
- Burov, E.B., Kogan, M.G., 1990. Gravitational–mechanical model of the continental plate collision in Tien Shan region. *Doklady Akademii Nauk, Physics of the Solid Earth* 313 (6), 439–1444.
- Burov, E.B., Molnar, P., 1998. Gravity anomalies over the Ferghana Valley (Central Asia) and intracontinental deformation. *Journal of Geophysical Research* 103, 18137–18152.
- Burov, E.B., Kogan, M.G., Lyon-Caen, H., Molnar, P., 1990. Gravity anomalies, the deep structure, and dynamic processes beneath the Tien Shan. *Earth and Planetary Science Letters* 96, 367–383.
- Burov, E.B., Lobkovsky, L.I., Cloetingh, S., Nikishin, A.M., 1993. Continental lithosphere folding in Central Asia (Part II): constraints from gravity and topography. *Tectonophysics* 226, 73–87.
- Burtman, V.S., 1975. Structural geology of the Variscan Tien Shan, USSR. *American Journal of Science* 272A, 157–186.
- Bushenkova, N., Tychkov, S., Koulakov, I., 2002. Tomography on PP-P waves and its application for investigation of the upper mantle in Central Siberia. *Tectonophysics* 358, 57–76.
- Buslov, M.M., Zykin, V.S., Novikov, I.S., Delvaux, D., 1999. Cenozoic history of the Chuya basin (Gorny Altai): structure and geodynamics. *Russian Geology and Geophysics* 40 (12), 1687–1701.
- Buslov, M.M., Klerkx, J., Abdрахmatov, K., Delvaux, D., Batalaev, V.Yu., Kuchai, O.A., Dehandschutter, B., Muraliev, A., 2003a. Recent strike–slip deformation of the northern Tien Shan. *Geological Society, London, Special Publications* 210, 53–64.
- Buslov, M.M., Watanabe, T., Smirnova, L.V., Fujiwara, Y., Iwata, K., De Grave, J., Semakov, N.N., Travin, A.V., Kirjanova, A.P., Kokh, D.A., 2003b. Role of strike–slip faulting in late Paleozoic–Early Mesozoic tectonics and geodynamics of the Altai–Sayan, and Kazakhstan regions. *Russian Geology and Geophysics* 44, 47–71.
- Buslov, M.M., Fujiwara, Y., Semakov, N.N., 2004a. Late Paleozoic–Early Mesozoic geodynamics of Central Asia. *Gondwana Research* 7, 791–808.
- Buslov, M.M., Watanabe, T., Fujiwara, Y., Iwata, K., Smirnova, L.V., Safonova, I.Yu., Semakov, N.N., Kiryanova, A.P., 2004b. Late Paleozoic faults of the Altai region, Central Asia: tectonic pattern and model of formation. *Journal of Asian Earth Sciences* 23, 655–671.
- Buslov, M.M., De Grave, J., Batalaeva, E.A.V., Batalaev, V.Yu., 2007. Cenozoic tectonic and geodynamic evolution of the Kyrgyz Tien Shan Mountains: a review of geological, thermochronological and geophysical data. *Journal of Asian Earth Sciences* 29, 205–214.
- Calais, E., Vergnolle, M., Sankov, V., Likhnev, A., Miroshnichenko, A., Amarjargal, S., Deverchere, J., 2003. GPS measurements of crustal deformation in the Baikal–Mongolia area (1994–2002): implications for current kinematics of Asia. *Journal of Geophysical Research* 108 (B10), 2501.
- Calais, E., Dong, L., Wang, M., Shen, Z., Vergnolle, M., 2006. Continental deformation in Asia from a combined GPS solution. *Geophysical Research Letters* 33, L24319.
- Caporali, A., 2000. Buckling of the lithosphere in western Himalaya: constraints from gravity and topography data. *Journal of Geophysical Research* 105 (B2), 3103–3113.
- Carroll, A.R., Graham, S.A., Hendrix, M.S., Ying, D., Zhou, D., 1995. Late Paleozoic tectonic amalgamation of northwestern China: sedimentary record of the northern Tarim, northwestern Turpan, and southern Junggar Basins. *Geological Society of America Bulletin* 107 (5), 571–594.
- Champagnac, J.-D., Molnar, P., Sue, C., Herman, F., 2012. Tectonics, climate, and mountain topography. *Journal of Geophysical Research* 117, B02403.
- Chang, H., Ao, H., An, Z., Fang, X., Song, Y., Qiang, X., 2012a. Magnetostatigraphy of the Serkuli Basin indicates Pliocene (3.2 Ma) activity of the middle Altyn Tagh Fault, northern Tibetan Plateau. *Journal of Asian Earth Sciences* 44, 169–175.
- Chang, J., Qiu, N., Li, J., 2012b. Tectono-thermal evolution of the northwestern edge of the Tarim basin in China: constraints from apatite (U–Th)/He thermochronology. *Journal of Asian Earth Sciences* 61, 187–198.
- Chedia, O.K., 1986. Morphology and Neotectonics of the Tien-Shan. Ilim Publications, Frunze (Bishkek), Kyrgyzstan (313 pp. (in Russian)).
- Cloetingh, S., Burov, E.B., 2011. Lithospheric folding and sedimentary basin evolution: a review and analysis of formation mechanisms. *Basin Research* 23 (3), 257–290.
- Cloetingh, S., Ziegler, P.A., 2007. Tectonic Models for the Evolution of Sedimentary Basins. In: Watts, A.B., Schubert, G. (Eds.), *Treatise on Geophysics*, 6. Elsevier, Amsterdam, pp. 486–611.
- Cloetingh, S., Burov, E.B., Poliakov, A., 1999. Lithospheric folding: primary response to compression? (from central Asia to Paris basin). *Tectonics* 18, 1064–1083.
- Cloetingh, S., Burov, E., Beekman, F., Amdeweg, B., Andriessen, P.A.M., Garcias-Castellanos, D., de Vicente, G., Vegas, R., 2002. Lithospheric folding in Iberia. *Tectonics* 21 (5), 1041.
- Cobbold, P.R., Davy, P., Gapais, D., Rossello, E.A., Sadybakasov, E., Thomas, J.C., Tondji Biyo, J.J., Urreiztieta, M., 1993. Sedimentary basins and crustal thickening. *Sedimentary Geology* 86, 77–89.
- Cobbold, P.R., Sadybakasov, E., Thomas, J.C., 1996. Cenozoic compression and basin development, Kyrgyz Tianshan, Central Asia. In: Roure, F., Ellouz, N., Shein, V.S., Skvortsov, I.I. (Eds.), *Geodynamic evolution of sedimentary basins*, Editions Technip, Paris, pp. 181–202.
- Cunningham, D., 2001. Cenozoic normal faulting and regional doming in the southern Hangay region, Central Mongolia: implications for the origin of the Baikal rift province. *Tectonophysics* 331, 145–411.
- Cunningham, W.D., Windley, B.F., Dorjnamjaa, D., Badamgarov, G., Saandar, M.A., 1996. A structural transect across the Mongolian Western Altai: active transpressional mountain building in Central Asia. *Tectonics* 15 (1), 142–156.
- De Batist, M., Imbo, Y., Vermeesch, P., Klerkx, J., Giralt, S., Delvaux, D., Linier, V., Beck, C., Kalugin, I., Abdрахmatov, K.E., 2002. Bathymetry and sedimentary environments of Lake Issyk-Kul: a large, high-altitude, tectonic lake. *NATO Science Series IV. Earth and Environmental Science* 13, 101–121.
- De Grave, J., Van den haute, P., 2002. Denudation and cooling of the Lake Teletskoye region in the Altai Mountains (South Siberia) as revealed by apatite fission-track thermochronology. *Tectonophysics* 349, 145–159.
- De Grave, J., Buslov, M.M., Van den haute, P., 2007a. Distant effects of India–Eurasia convergence and Mesozoic intracontinental deformation in Central Asia: constraints from apatite fission-track thermochronology. *Journal of Asian Earth Sciences* 29, 188–204.
- De Grave, J., Buslov, M.M., Van den haute, P., Dehandschutter, B., Delvaux, D., 2007b. Meso-Cenozoic Evolution of Mountain Range–Intramontane Basin Systems in the Southern Siberian Altai Mountains by Apatite Fission-Track thermochronology. In: Lacombe, O., Lavé, J., Roure, F.M., Verges, J. (Eds.), *Thrust Belts and Foreland Basins - From fold kinematics to hydrocarbon systems*. Frontiers in Earth Sciences, XXIV. Springer, pp. 457–470.
- De Grave, J., Buslov, M.M., Van den Haute, P., Metcalf, J., Dehandschutter, B., McWilliams, M.O., 2009. Multi-method chronometry of the Teletskoye graben and its basement, Siberian Altai Mountains: new insights on its thermotectonic evolution. *Geological Society, London, Special Publications* 324, 237–259.
- De Grave, J., Glorie, S., Buslov, M.M., Izmer, A., Fournier-Carrie, A., Batalaev, V.Y., Vanhaecke, F., Elburg, M., Van den haute, P., 2011. The Thermo-tectonic history of the Sang-Kul plateau, Kyrgyz Tien Shan: constraints by apatite and titanite thermochronometry and zircon U/Pb dating. *Gondwana Research* 20, 745–763.
- Dehandschutter, B., 2001. Study of the structural evolution of continental basins in Altai, Central Asia. PhD. Thesis dissertation, Free University of Brussels. 211 pp.
- Dehandschutter, B., Vysotsky, E., Delvaux, D., Klerkx, J., Buslov, M.M., Seleznev, V.S., De Batist, M., 2002. Kinematic evolution of the Teletsk Graben. *Tectonophysics* 351, 139–168.
- Delvaux, D., 2012. Release of Program Win-Tensor 4.0 for Tectonic Stress Inversion: Statistical Expression of Stress Parameters. *Geophysical Research Abstracts*, vol. 14. EGU General Assembly, Vienna (EGU2012-5899). Program available at: <http://users.skynet.be/damien.delvaux/Tensor/tensor-index.html>.
- Delvaux, D., Sperner, B., 2003. Stress tensor inversion from fault kinematic indicators and focal mechanism data: the TENSOR program. In: new insights into structural interpretation and modelling. *Geological Society of London, Special Publication* 212, 75–100.
- Delvaux, D., Fernandez-Alonso, M., Klerkx, J., Kuzmin, A., Matton, C., Selegei, V., Theunissen, K., Vysotskii, E., 1995a. Evidences for active tectonics in Lake Teletskoye (Gorny–Altai, South–Siberia). *Russian Geology and Geophysics* 36 (10), 100–112.
- Delvaux, D., Moeyers, R., Stapel, G., Melnikov, A., Ermikov, V., 1995b. Paleostress reconstructions and geodynamics of the Baikal region, Central Asia. Part I: Paleozoic and Mesozoic pre-rift evolution. *Tectonophysics* 252, 61–101.
- Delvaux, D., Theunissen, K., Van der Meer, R., Berzin, N., 1995c. Formation dynamics of the Gorno-Altaiian Chuya–Kurai depression in Southern Siberia: paleostress, tectonic and climatic control. *Russian Geology and Geophysics* 36 (10), 26–45.
- Delvaux, D., Moeyers, R., Stapel, G., Petit, C., Levi, K., Miroshnichenko, A., Ruzhich, V., Sankov, V., 1997. Paleostress reconstructions and geodynamics of the Baikal region, Central Asia. Part II: Cenozoic rifting. *Tectonophysics* 282, 1–38.

- Delvaux, D., Abdрахmatov, K.E., Strom, A.L., 2001. Landslides and surface breaks of the 1911 Ms 8.2 Kemin earthquake, Kyrgyzstan. *Russian Geology and Geophysics* 42 (10), 1167–1177.
- Dergachev, A.A., 2008. Detailed seismicity mapping of the Altai–Sayan zone using large averaging areas. *Russian Geology and Geophysics* 49, 963–970.
- Dergunov, A.B., 1972. Quaternary compression and extension structures in the Eastern Altai. *Geotectonica* 3, 99–100 (in Russian).
- Deviatkin, E.V., 1965. Cenozoic Sediments and Neotectonics of South-Eastern Altai. *Acad. Sci USSR, Geol. Int. Transactions*, 126. Nauka, Moscow 234 pp. (in Russian).
- Deviatkin, E.V., 1981. The Cenozoic of Inner Asia. *Nauka, Moscow* (196 pp. (in Russian)).
- Dobretsov, N.L., Buslov, M.M., 2007. Late Cambrian–Ordovician tectonics and geodynamics of Central Asia. *Russian Geology and Geophysics* 48, 71–82.
- Dobretsov, N.L., Vladimirov, A.G. (Eds.), 2001. Continental Growth in the Phanerozoic: Evidence from Central Asia. *Geology, Magmatism and Metamorphism in the Western part of Altai–Sayan Fold Region: IGCP-420, 3rd Workshop. UIGGM, Siberian Branch of the Russian Academy of Science, Field Excursion Guide, Novosibirsk*.
- Dobretsov, N.L., Buslov, M.M., Delvaux, D., Berzin, N.A., Ermikov, V.D., 1996. Mesozoic tectonics of the Central Asian orogenic belt: collision of lithospheric plates and mantle plume. *International Geology Review* 38, 430–466.
- Dricker, I.G., Roecker, S.W., Vinnik, L.P., Rogozhin, E.A., Makeyeva, L.I., 2002. Upper-mantle anisotropy beneath the Altai–Sayan region of central Asia. *Physics of the Earth and Planetary Interiors* 131, 205–223.
- Duchkov, A.D., Sokolova, S., 1974. The heat flow in the central areas of the Altai–Sayan region. *Soviet Geology and Geophysics* 15 (8), 88–97.
- Duchkov, A.D., Schwartsman, Yu.G., Sokolova, L.S., 2001. Deep heat flow in the Tien Shan: advances and drawbacks. *Russian Geology and Geophysics* 42, 1436–1452.
- Duchkov, A.D., Rychkova, K.M., Lebedev, V.I., Kamenskii, I.L., Sokolova, L.S., 2010. Estimation of heat flow in Tuva from data on helium isotopes in thermal mineral springs. *Russian Geology and Geophysics* 51, 209–219.
- Dunne, W.M., Hancock, P.L., 1994. Paleostress analysis of small-scale brittle structures. In: Hancock, P.L. (Ed.), *Continental Deformation*. Pergamon, Oxford, pp. 101–120.
- Egorov, A.S., Chistyakov, D.N., 2003. Deep structure of the basement of the West Siberian Platform and its folded surroundings. *Russian Geology and Geophysics* 44, 99–114.
- Erofeev, V.S., 1969. Paleogene and Neogene geological history of the southern margin of Altai. *Nauka, Alma-Ata* (167 pp. (in Russian)).
- Fang, S., Song, Y., Ong, Y., Jia, C., Guo, Z., Zhang, Z., Liu, L., 2007. Timing of Cenozoic intense deformation and its implications for petroleum accumulation, northern margin of Tianshan orogenic belt, Northwest China. *Earth Science Frontiers* 14 (2), 205–214.
- Fortuna, A.B., 1993. Detailed Seismic Profiling of the Issyk-Kul Depression. Ilim Publications, Bishkek (in Russian).
- Gao, J., Klemm, R., Qian, Q., Zhang, X., Li, J., Jiang, T., Yang, Y., 2011. The collision between the Yili and Tarim blocks of the Southwestern Altaids: geochemical and age constraints of a leucogranite dike crosscutting the HP–LT metamorphic belt in the Chinese Tianshan Orogen. *Tectonophysics* 499, 118–131.
- Gerbault, M., Burov, E.B., Poliakov, A., Daignières, M., 1999. Do faults trigger folding in the lithosphere? *Geophysical Research Letters* 26 (2), 271–274.
- Ghose, S., Mellors, R.J., Korjenkov, A.M., Hamburger, M.W., Pavlis, T.L., Pavlis, G.L., Omuraliev, M., Mamyrov, E., Muraliev, A.R., 1997. The Ms = 7.3 1992 Sausamyr, Kyrgyzstan, earthquake in the Tien Shan: 2. Aftershock focal mechanisms and surface deformation. *Bulletin of the Seismological Society of America* 87 (1), 23–38.
- Glorie, S., De Grave, J., Buslov, M.M., Zhimulev, F.I., Stockli, D.F., Batalev, V.Y., Izmer, A., Van den Haute, P., Vanhaecke, F., Elburg, M.A., 2011. Tectonic History of the Kyrgyz South Tien Shan (Atbashi–Inylchek) Suture Zone: The Role of Inherited Structures During Deformation–Propagation. *Tectonics* 30, TC6016.
- Glorie, S., De Grave, J., Delvaux, D., Buslov, M.M., Zhimulev, F.I., Elburg, M.A., Van den Haute, P., 2012. Tectonic history of the Irtysh shear zone (NE Kazakhstan): new constraints from zircon U/Pb dating, apatite fission track dating and palaeostress analysis. *Journal of Asian Earth Sciences* 45, 138–149.
- Goldin, S.V., Kuchai, O.A., 2007. Seismic strain in the Altai–Sayan active seismic area and elements of collisional geodynamics. *Russian Geology and Geophysics* 48, 537–557.
- Goldin, S.V., Timofeev, V.Yu., Ardyukov, D.G., 2005. Fields of the earth's surface displacement in the Chuya earthquake zone in Gornyi Altai. *Doklady Earth Sciences* 405A, 1408.
- Heermance, R.V., Chen, J., Burbank, D.W., Miao, J., 2008. Temporal constraints and pulsed Late Cenozoic deformation during the structural disruption of the active Kashi foreland, northwest China. *Tectonics* 27, TC6012.
- Hendrix, M.S., Graham, S.A., Carroll, A.R., Sobel, E.R., McKnight, C.L., Schuelein, B.J., Wang, Z., 1992. Sedimentary record and climatic implications of recurrent deformation in the Tien Shan: evidence from Mesozoic strata of the north Tarim, south Junggar, and Turpan basins, northwest China. *Geological Society of America Bulletin* 104, 53–79.
- Huang, G., Charlesworth, H., 1989. A FORTRAN-77 program to separate a heterogeneous set of orientations into subsets. *Computer and Geosciences* 15, 1–7.
- Hunt, G., Muhlhaus, H., Hobbs, B., Ord, A., 1996. Localized folding of viscoelastic layers. *Geologische Rundschau* 85, 58–64.
- Jolivet, M., Ritz, J.-F., Vassallo, R., Larroque, C., Braucher, R., Todbileg, M., Chauvet, A., Sue, C., Arnaud, N., De Vicente, R., Arzhanikova, A., Arzhanikov, S., 2007. Mongolian summits: an uplifted, flat, old but still preserved erosion surface. *Geology* 35 (10), 871–874.
- Kalinin, V.A., Moiseeva, E. G., 1975. Geological map of URSS, sheet M-(44), 45 Ust-Kamenogorsk. 1:1,000,000 geological map, Ministry of Geology of the USSR.
- Kashik, S.A., Mazilov, V.N., 1994. Main stages and palaeogeography of Cenozoic sedimentation in the Baikal rift system (Eastern Siberia). *Bulletin des Centres de Recherches Exploration-Production Elf-Aquitaine* 18, 453–462.
- Kumar, P., Yuan, X., Kind, R., Kosarev, G., 2005. The lithosphere–asthenosphere boundary in the Tien Shan–Karakoram region from S receiver functions: evidence for continental subduction. *Geophysical Research Letters* 32, L07305.
- Le Pichon, X., Fournier, M., Jolivet, L., 1992. Kinematics, topography, shortening and extrusion in the India–Eurasia collision. *Tectonics* 11 (6), 1085–1098.
- Lefort, J.P., Agarwal, B.N.P., 1996. Gravity evidence for an Alpine buckling of the crust beneath the Paris Basin. *Tectonophysics* 258, 1–14.
- Leith, W., 1985. A mid-Mesozoic extension across Central Asia? *Nature* 313, 567–570.
- Li, C., Guo, Z., Dupont-Nivet, G., 2011. Late Cenozoic tectonic deformation across the northern foreland of the Chinese Tien Shan. *Journal of Asian Earth Sciences* 42, 1066–1073.
- Logatchev, N.A., 1993. History and geodynamics of the Lake Baikal rift in the context of the Southeastern Gorny Altai. *Russian Geology and Geophysics* 33 (4), 18–23.
- Lund, B., Townend, J., 2007. Calculating horizontal stress orientations with full or partial knowledge of the tectonic stress tensor. *Geophysical Journal International* 170, 1328–1335.
- Luzgin, B.M., Ruzanov, G.G., 1992. Characteristics of formation of Neogenic deposits in the Southeastern Gorny Altai. *Russian Geology and Geophysics* 33 (4), 18–23.
- Makarov, V.I., 2012. Compositional, structural, and geodynamic controls of the evolution of inter- and intramontane basins of the Tien Shan. *Russian Geology and Geophysics* 53, 367–375.
- Martinod, J., Davy, P., 1992. Periodic instabilities during compression of the Lithosphere. 2. Deformation modes from an analytical perturbation method. *Journal of Geophysical Research* 97 (B2), 1999–2014.
- Martinod, J., Davy, P., 1994. Periodic instabilities during compression of the Lithosphere. 2. Analogue experiments. *Journal of Geophysical Research* 99 (B6), 12057–12069.
- Meade, B.J., Hager, B.H., 2001. The current distribution of deformation in western Tien Shan from block models constrained by geodetic data. *Russian Geology and Geophysics* 42 (10), 1538–1549.
- Mekhed, L.P., Shamshikov, I.F., 1987. Techniques and results of reconnaissance seismic surveys in the Zaisan basin. *Izvestia Akademii Nauk Kazakh SSR Seria Geologicheskaya* 5, 80–87 (in Russian).
- Mikolaichuk, A.V., 2000. The structural position of thrusts in the recent orogen of the Central Tien Shan. *Russian Geology and Geophysics* 41 (7), 929–939.
- Molnar, P., England, P., 1990. Late Cenozoic uplift of mountain ranges and global climate change: chicken or egg? *Nature* 346 (6279), 29–34.
- Mossakovsky, A.A., Dergunov, A.B., 1985. The Caledonides of Kazakhstan, Siberia and Mongolia: a review of structure, development history, and paleotectonic environments. In: Gee, D.G., Sturt, B.A. (Eds.), *The Caledonide Orogen–Scandinavia and related areas*. Wiley.
- Neil, E.A., Houseman, G.A., 1997. Geodynamics of the Tarim basin and the Tien Shan in Central Asia. *Tectonics* 16 (4), 571–584.
- Nikishin, A.M., Cloetingh, S., Lobkovsky, L.I., Burov, E.B., Lankreijer, A.C., 1993. Continental lithosphere folding in Central Asia (Part I): constraints from geological observations. *Tectonophysics* 226, 59–72.
- Nissen, E., Emmerson, B., Funning, G.J., Mistrukov, A., Parsons, B., Robinson, D.P., Rogozhin, E., Wright, T.J., 2007. Combining InSAR and seismology to study the 2003 Siberian Altai earthquakes – dextral strike-slip and anticlockwise rotations in the northern India–Eurasia collision zone. *Geophysical Journal International* 169, 216–232.
- Novikov, I.S., Delvaux, D., Agatova, A.R., 1998. Neotectonics of the Kurai Ridge (Gorny–Altai). *Russian Geology and Geophysics* 39 (7), 970–977.
- Novikov, I.S., Emanov, A.A., Leskova, E.V., Batalev, V.Yu., Rybin, A.K., Bataleva, E.A., 2008. The system of neotectonic faults in southeastern Altai: orientations and geometry of motion. *Russian Geology and Geophysics* 49, 859–867.
- Omuraliev, M.O., 1979. Natural resources of the Kyrgyz republic, Tectonic map, 1:500,000, sheets K-43-b and K-44-A. Institute of Seismology, Kyrgyz Academy of Sciences.
- Omuraliev, M.O., 1980. Natural resources of the Kyrgyz republic, Neotectonic map, 1:500,000, sheets K-43-b and K-44-A. Institute of Seismology, Kyrgyz Academy of Sciences.
- Omuraliev, A., Nakajima, J., Hasegawa, A., 2009. Three-dimensional seismic velocity structure of the crust beneath the central Tien Shan, Kyrgyzstan: implications for large- and small-scale mountain building. *Tectonophysics* 465, 30–44.
- Pubellier, M., 2008. Structural map of Easter Eurasia – Evolution of crustal blocks and orogenic belts through time. 1:12,500,000, Commission for the Geological Map of the World, Paris, France.
- Reigber, Ch., Michel, G.W., Galas, R., Angermann, D., Klotz, J., Chen, J.Y., Papschev, A., Arslanov, R., Tzurkov, V.E., Ishanov, M.C., 2001. New space geodetic constraints on the distribution of deformation in Central Asia. *Earth and Planetary Science Letters* 191, 157–165.
- Rogozhin, E.A., Leontyev, A.N., 1992. The Zaisan Earthquake of 1990: Geologic data. *Doklady Russian Academy of Sciences, Earth Sciences* 325 (5), 106–112.
- Rogozhin, E.A., Ovsyuchenko, A.N., Geodakov, A.R., Platonova, S.G., 2003. A strong earthquake of 2003 in Gorny Altai. *Russian Journal of Earth Sciences* 5 (6), 439–454.
- Rudoy, A.N., 2002. Glacier-dammed lakes and geological work of glacial superfoods in the Late Pleistocene, South Siberia, Altai Mountains. *Quaternary International* 87 (1), 119–140.
- Sadybakazov, E., 1990. Neotectonics of High Asia. *Nauka, Moscow* (176 pp. (in Russian)).
- Sankov, V.A., Miroshnichenko, A.I., Levi, K.G., Lukhnev, A., Melnikov, A.I., Delvaux, D., 1997. Cenozoic tectonic stress field evolution in the Baikal Rift Zone. *Bulletin des Centres de Recherches Exploration-Production Elf-Aquitaine* 21 (2), 435–455.
- Scharer, K.M., Burbank, D.W., Chen, J., Weldon, R.J., Rubin, C., Zhao, R., Shen, J., 2004. Detachment folding in the Southwestern Tien Shan–Tarim foreland, China: shortening estimates and rates. *Journal of Structural Geology* 26, 2119–2137.

- Schlupp, A., 1996. Néotectonique de la Mongolie occidentale analysée à partir de données de terrain, sismologiques et satellitaires. Ph.D Thesis, University L. Pasteur, EOPG, Strasbourg, France, 172 pp.
- Schwartzman, Yu.G., 1991. Thermal energetics of bowels of the Earth. In: Laverov, N.P., et al. (Ed.), *Current geodynamics of the lithosphere of Tien Shan*. Nauka, Moscow (192 pp. (in Russian)).
- Sengör, A.M.C., Natal'in, B.A., Burtam, V.S., 1993. Evolution of the Altaid tectonic collage and Paleozoic crustal growth in Eurasia. *Nature* 364, 299–307.
- Sokolova, L.S., Duchkov, A.D., 2008. Heat flow in the Altai–Sayan area: new data. *Russian Geology and Geophysics* 49, 940–950.
- Sokoutis, D., Burg, J.-P., Bonini, M., Corti, G., Cloetingh, S., 2005. Lithospheric-scale structures from the perspective of analogue continental collision. *Tectonophysics* 406, 1–15.
- Stephenson, R.A., Cloetingh, S.A.P.L., 1991. Some examples and mechanical aspects of continental lithospheric folding. *Tectonophysics* 188, 27–37.
- Stephenson, R.A., Lambeck, K., 1985. Isostatic response of the lithosphere with in-plane stress: application to Central Australia. *Journal of Geophysical Research* 90, 8581–8588.
- Sun, J., Zhu, R., Bowler, J., 2004. Timing of the Tianshan Mountains uplift constrained by magnetostratigraphic analyses of molasses deposits. *Earth and Planetary Science Letters* 219, 239–253.
- Thomas, J.-C., Perroud, H., Cobbold, P.R., Bazhenov, M.L., Burtman, V.S., Chuvin, A., Sadybakazov, E., 1993. A paleomagnetic study of Tertiary formations from the Kyrgyz Tien-Shan and its tectonic implications. *Journal of Geophysical Research* 98 (B6), 9571–9589.
- Thomas, J.C., Lanza, R., Kazansky, A., Zykina, V., Semakov, N., Mitrokhin, D., Delvaux, D., 2002. Paleomagnetic study of Cenozoic sediments from the Zaisan basin (SE Kazakhstan) and the Chuya depression (Siberian Altai): tectonic implications for central Asia. *Tectonophysics* 351, 119–138.
- Thompson, S.C., Weldon, R.J., Rubin, C.M., Abdrakhmatov, K., Molnar, P., Berger, G.W., 2002. Late Quaternary slip rates across central Tien Shan, Kyrgyzstan, central Asia. *Journal of Geophysical Research* 107, 2203.
- Tibaldi, A., Graziotto, E., Forcella, F., Gapich, V.H., 1997. Morphotectonic indicators of Holocene faulting in Central Tien Shan, Kazakhstan, and geodynamic implications. *Journal of Geodynamics* 23 (1), 23–45.
- Timofeev, V.Yu., Ardyukov, D.G., Calais, E., Duchkov, A.D., Zapreeva, E.A., Kazantsev, S.A., Roosbeek, F., Bruyninx, C., 2006. Displacement fields and models of current motion in Gorny Altai. *Russian Geology and Geophysics* 47 (8), 915–929.
- Trofimov, A.K., Udalov, H.P., Utken, H.G., Fortuna, A.B., Chediya, O.K., Yazovskii, B.M., 1976. *Cenozoic Geology of the Chu Basin and Surrounding Mountains*. Academia Nauk CCCP, Leningrad, pp. 1–128 (in Russian).
- Tursungasiev, B.T., Petrov, O.B., 2008. Geological map of the Kyrgyz republic. 1:500,000. State agency for geology and mineral resources of the government of Kyrgyz republic.
- Tychkov, S.A., Kuchai, O.A., Bushenkova, N.A., Bragin, V.D., Kalmetieva, Z.A., 2008. Current crustal deformation in the northern Tien Shan: GPS and seismological data. *Russian Geology and Geophysics* 49, 280–290.
- Van der Beek, P.A., Delvaux, D., Andriessen, P.A.M., Levi, K.G., 1996. Early Cretaceous denudation related to convergent tectonics in the Baikal region, SE Siberia. *Geological Society of London* 153, 515–523.
- Vassallo, R., Jolivet, M., Ritz, J.-F., Braucher, R., Larroque, C., Sue, C., Toddbileg, M., Javkhlanbold, D., 2007. Uplift age and rates of the Gurvan Bogd system (Gobi–Altay) by apatite fission track analysis. *Earth and Planetary Science Letters* 259, 333–346.
- Vergnolle, M., Calais, E., Dong, L., 2007. Dynamics of continental deformation in Asia. *Journal of Geophysical Research* 112, B11403.
- Vermeesch, P., Poort, J., Duchkov, A.D., Klerkx, J., De Batist, M., 2004. Lake Issyk-Kul (Tien Shan): unusually low heat flow in an active intramontane basin. *Russian Geology and Geophysics* 45, 616–625.
- Vinnik, L.P., Reigber, C., Aleshin, I.M., Kosarev, G.L., Kaban, M.K., Oreshin, S.I., Roecker, S.W., 2004. Receiver function tomography of the central Tien Shan. *Earth and Planetary Science Letters* 225, 131–146.
- Wang, Y., Deng, T., Flynn, L., Wang, X., Yin, A., Xu, Y., Parker, W., Lochner, E., Zhang, C., Biasatti, D., 2012. Late Neogene environmental changes in the central Himalaya related to tectonic uplift and orbital forcing. *Journal of Asian Earth Sciences* 44, 62–76.
- Weissel, J., Anderson, R.N., Geller, C., 1980. Deformation of the Indo-Australian plate. *Nature* 287, 284–291.
- Windley, B.F., Alexeev, D., Xiao, W., Kršner, A., Badarch, G., 2007. Tectonic models for accretion of the Central Asian Orogenic Belt. *Journal of the Geological Society of London* 164, 31–47.
- Xie, Fu-Ren, Zhang, Shi-Min, Dou, Su-Qin, Cui, Xiao-Feng, Sai-Bing, S.H.U., 1999. Evolution characteristics of Quaternary tectonic stress field in the north and east margin of Qinghai–Xizang plateau. *Acta Seismologica Sinica* 12 (5), 550–561.
- Yang, Y., Liu, M., 2002. Cenozoic deformation of the Tarim plate and the implications for mountain building in the Tibetan Plateau and the Tien Shan. *Tectonics* 21 (6), 1059.
- Yuan, W., Carter, A., Dong, J., Bao, Z., An, Y., Guo, Z., 2006. Mesozoic–Tertiary exhumation history of the Altai Mountains, northern Xinjiang, China: new constraints from apatite fission track data. *Tectonophysics* 412, 183–193.
- Zhalkovskii, N.D., Kuchai, O.A., Muchnaya, V.I., 1995. Seismicity and some characteristics of the stress state of the Earth's crust in the Altai–Sayan region. *Russian Geology and Geophysics* 36, 16–25.
- Zheng, H., Powell, C. McA., An, Z., Zhou, J., Dong, G., 2000. Pliocene uplift of the northern Tibet Plateau. *Geology* 28 (8), 715–718.
- Zuber, M.T., 1987. Compression of oceanic lithosphere: an analysis of intraplate deformation in the Central Indian Basin. *Journal of Geophysical Research* 92, 4817–4825.
- Zubovich, A.V., Trapeznikov, Yu.A., Bragin, V.D., Mosienko, O.I., Schelochkov, G.G., Rybin, A.K., Batalev, V.Yu., 2001. Deformation field, deep crustal structure, and spatial seismicity distribution in the Tien Shan. *Russian Geology and Geophysics* 42, 1550–1557.
- Zykin, V.S., Kazansky, A.Y., 1995. Main problems of stratigraphy and paleomagnetism of Cenozoic (PreQuaternary) deposits of Chuya depression of Gorny Altai. *Russian Geology and Geophysics* 35 (10), 75–90.